Studies in Hydroelastodynamics: Singing and Swimming

Thesis advisor

L. Mahadevan

Author

Aryesh Mukherjee

Studies in Hydroelastodynamics: Singing and Swimming

Abstract

In this thesis we describe two instances of the nonlinear interaction between a fluid and an elastic solid to mimic or explain some phenomenon seen in nature. We focus on the phenomena of singing of small song birds and swimming of small fish. Song birds show a versatile range of tones and compositions that have highly complex spectral structure, while fish cut through water with amazing ease. The complexity of the Navier Stokes Equations that describe the fluid coupled with large deformation elasticity equations, makes analytic attempts intractable. Hence experiments were carried out with simple physical models to explain these observations. In the first case a cylindrical elastic tube (2.5cm long, 2.5mm diameter) was used to model the vocal organ, the syrinx, of a song bird. Muscle action was mimicked using a linear motor that implemented a squeezing action and the action of the lungs was modeled by a constant source of air flow. The combined fluid-elastic system behaved like a nonlinear dynamical system and produced sound under certain conditions of external parameters. Moreover the structure of the sound created depended sensitively on the control parameters, which in this case was dominated by the position of the linear motor. The motor was dynamically controlled to produce a range of songs from simple tonal ones of the Vireo to the complex chaotic songs of the Zebra Finch. In the second instance, a cantilever (5cm long, 1cm wide)suspended between and driven

by magnetic coils arranged in an anti-Helmholtz configuration, was used to mimic the dynamics of the caudal fin of a small fish. Three different gaits were observed as a function of the control parameter, the drive frequency. One of these gaits maximized thrust and hydrodynamic efficiency, and velocities unto 6 body lengths per second were measured.

Contents

Acknowledgments

My love affair with science has been a long one. And without the help and support of my family and friends I would not have realized my dream of perhaps making this affair a life long one. My training started early as my parents motivated and encouraged me to pursue my goals with passion and conviction. They taught me the value of hard work, humility and honesty and their wisdom has guided me through the darkest of times. Under my thesis adviser Prof. L. Mahadevan I finally began to realize what science really was, and that is was a rich, creative almost artistic field. Maha opened my mind and taught me to ask questions, to think abstractly and to conceptualize. I am utterly grateful for his training and guidance. I am thankful to my committee members Prof. Wood and Prof. Olveczky for inspiring and encouraging me and making me better. And of course I have learnt an infinite amount from my friends and lab members. Their insightful questions and mind boggling research served as much motivation during the trying times of a Phd. However this is only the mental and I feel man is incomplete if he stays away from physical enterprises. This for me was my second love affair, with rocks and mountains. The sport of rock climbing has not only served to refresh my mind and sport continuously but has also been a source of great friendships. I am thankful to all my rock climbing friends for teaching me patience, endurance, empathy and perseverance. The lessons I have learnt from climbing have served me well and shaped me as a person over the course of my Phd.

To my parents.

Chapter 1

Introduction

Linear systems, although simple and elegant are restrictive and in a sense expensive, because they only exhibit one type of behavior. Non linear systems, often viewed as vexing and cumbersome, can resolve this issue by allowing different behaviors or modalities to exist in their phase space. Often it is possible to find a few parameters that can "tune" the behavior of the dynamical system, and sometimes linear behavior is exhibited within each of these phases. For example, as will be shown in Chapter 2, a simple cylindrical elastic tube can sustain different kinds of oscillations on its surface that couple to the surrounding fluid medium (in this case air) and create sound. We demonstrate that we can switch the behavior of the device with a simple one parameter control, moreover in each of these "phases" the fundamental frequency of the sound produced scales linearly with the control parameter.

Not all nonlinear systems exhibit many phase behavior, for example a diode is a nonlinear device that displays only one kind of behavior; there is a nonlinear relationship between the current and voltage, but no new phases are ever created. A driven

damped pendulum is a nonlinear dynamical system that displays two periodic behaviors, one in which the pendulum oscillates sinusoidally about its equilibrium position and another in which the pendulum exhibits 2π rotations about its axis. A prototypical nonlinear oscillator that has been studied analytically and used to model action potential in neurons is the Van der Pol oscillator. Mathematically it can be written as a second order differential equation with nonlinear damping, $\ddot{x} - \mu(1 - x^2)\dot{x} + x = 0$ [26] where x is the dynamical variable and μ controls the strength of the damping. For $\mu = 0$ the system is a simple harmonic oscillator, but for $\mu > 0$ the system exhibits limits cycles (self sustained oscillations) where energy is conserved. However for large values of x the system is damped. Hence such systems exhibit a sharp turn on behavior as soon as the effective damping coefficient $\mu(1 - x^2)$ becomes positive, but as soon as x becomes too large the damping becomes negative and the system slowly relaxes, before the damping becomes positive again and the system shows a sharp recovery. Such oscillations are called relaxation oscillations and have been used to model aspects of phonation in song birds.

Driven nonlinear systems can show even more complicated behavior; for example when driven strongly the system can oscillate at frequencies that are integer fractions of the driving frequency (known as period multiplication). One such system is the driven Duffing oscillator [13] described by, $\ddot{x} + \delta x - \beta x + \alpha x^3 = f \cot \omega t$ where δ, is the damping, β is the spring constant and α is a parameter that controls the strength of the nonlinearity. A physical system approximated by this equation is a simple bistable beam much like a hair clip and can be thought of a particle in a double well potential [13] . This system has three fixed points, two which are stable and one unstable. The

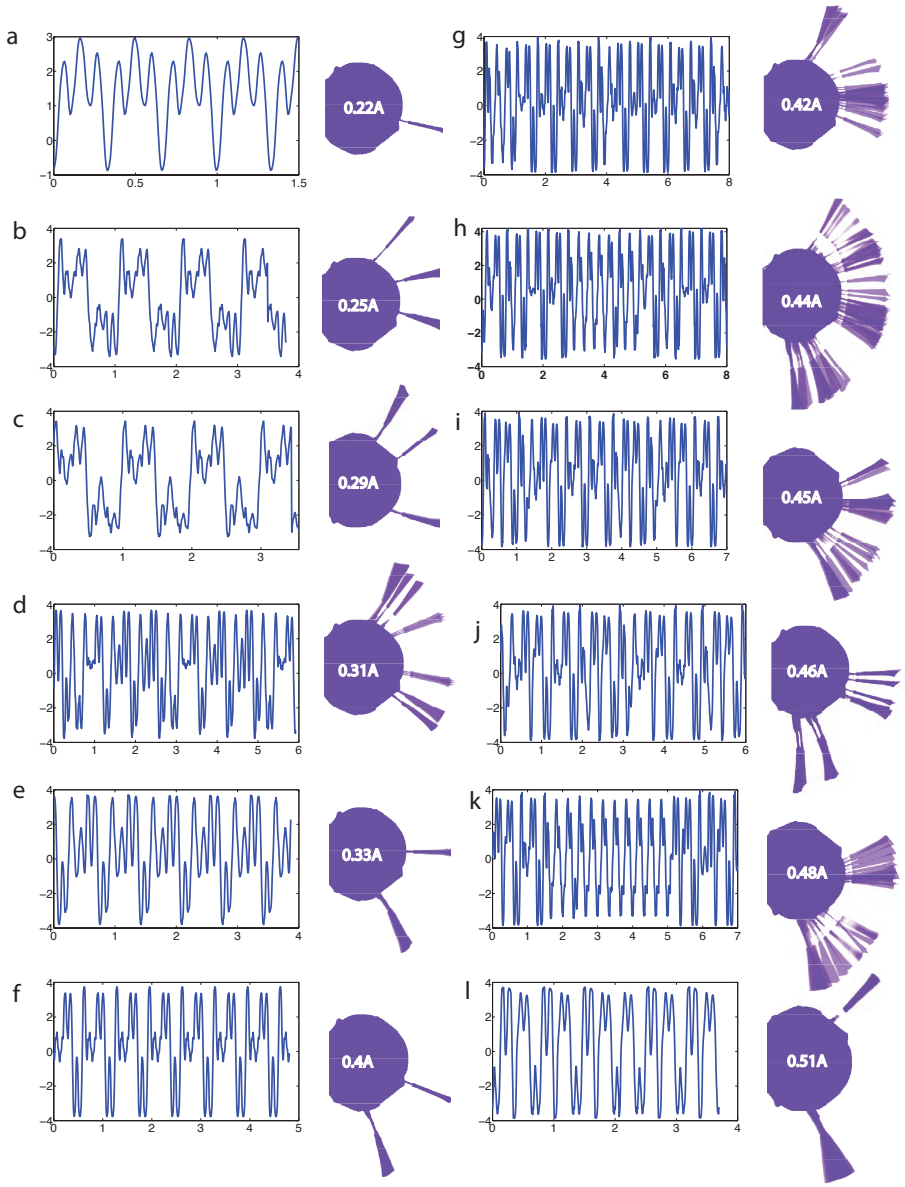

Figure 1.1: Nonlinear Dynamics of a bistable beam driven by a magnetic coil assembly. (a-l) show Stroboscopic Images of the oscillator as a function of drive current (input power). The strobing frequency and the drive frequency were set to 6.81 Hz, which was close to resonance observed at 8Hz. In (a) the power is low and the system oscillates with the same period as the drive. As the power is increased period multiplication is observed, first to a period three orbit, then to a period two orbit, then to apparently chaotic orbits and finally when the power is high a period two orbit was observed. The period two orbit corresponds to one in which the device flips back and forth between the two buckled states of the beam.

stable fixed points correspond to the two bistable states of the device, and the unstable fixed point is when the strip is completely flat. We studied such a system and observed many interesting behaviors (figures [1-2]).Figure [1] shows stroboscopic images of the oscillator as a function of drive power at a fixed drive frequency (close to resonance). In such an imaging technique a sequence of images of the oscillator taken at times spaced by T, (T=1/f, where f is the driving frequency) are superimposed on top of one another to give an idea of the dynamics. If only one image of the oscillator is seen, it can be inferred that its fundamental frequency is the same as the driving frequency. However, if multiple images are seen then the fundamental frequency is some fraction of the drive. In our system, for low amplitude the system oscillated in one of the wells, but as the power was increased period-2,3,5,7 oscillations were observed. For a drive current of 0.44A a chaotic like oscillation was observed. Figure[2a] shows a time series of a chaotic oscillation observed in this system. Figure[2b] shows a "strange attractor" in the phase space of the oscillator, confirming the chaotic nature of the time series. In nature we find chaotic oscillations in the songs of certain song birds, and this motivates one to study the esoteric dynamics of nonlinear dynamical systems.

In this work we wish to use nonlinear systems to understand and mimic complicated patterns we find in nature. Such phenomena are present everywhere and we restrict our attention to systems where the behavior is determined by the coupling of fluid systems with elastic systems. Fluid dynamics governed by the Navier Stokes equations is inherently nonlinear and displays a vast arrays of patterns most of which are too complicated to handle analytically. Elastic systems similarly are also nonlinear when the deformations imposed are large and can cause local buckling. In this

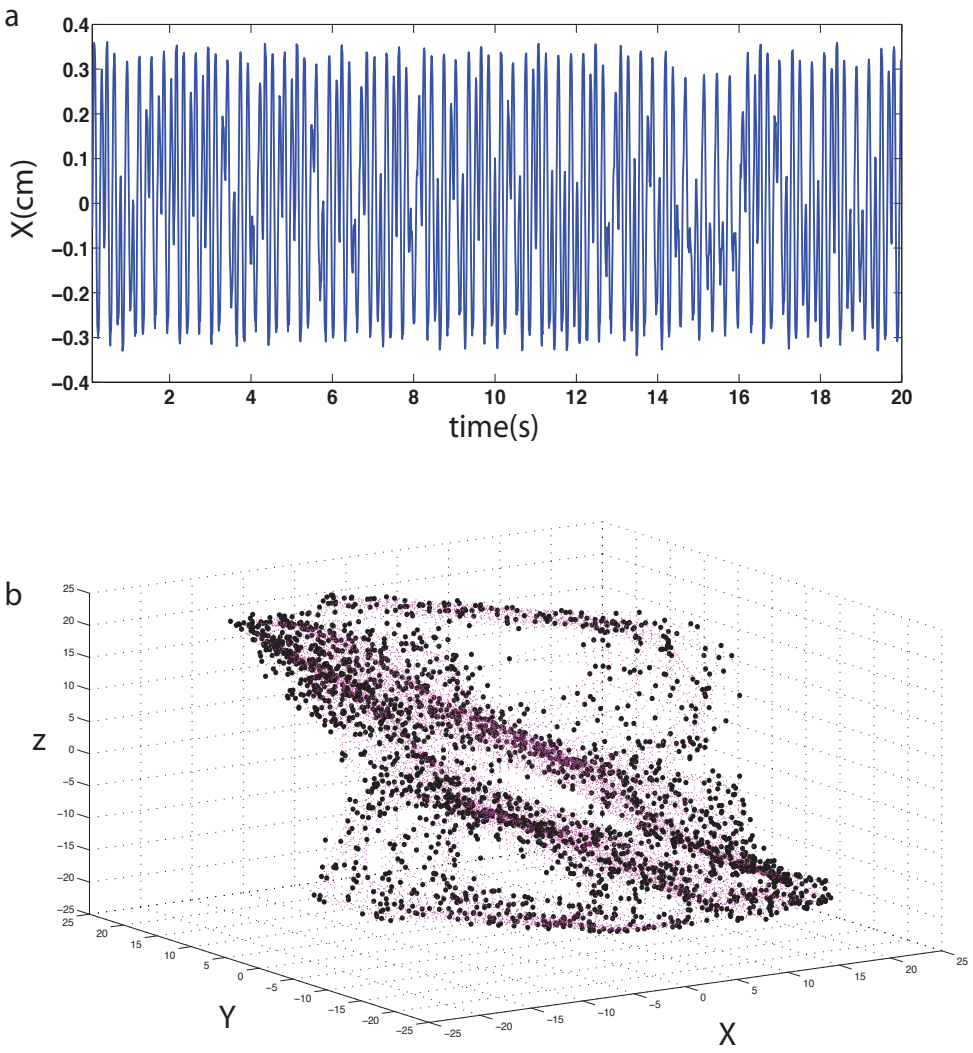

Figure 1.2: Observation of chaos in a driven bistable beam. (a) shows a time series of a chaotic orbit (figure [1h]). (b) Reconstructed phase space using delay coordinates shows a strange attractor. First given a time series $x_i = x(n\Delta t), n = 1, 2..., N$, where Δt is the sample time and N is the number of samples, we form a vector of time delayed coordinates i.e. find $X_i = (x_i, x_{i+m}, ...x_{i+(d-1)m})$, where m is an appropriate delay and d is the dimension of the embedding (in our case d=3). For specific values of m, a strange attractor is observed in the phase space. Here the attractors are the two buckled states of the elastic beam.

thesis we study the nonlinear interactions between a fluid flow and an elastic object. We restricted our attention to fluid flows where the Reynolds number (Re=LU/ν, where L is a length scale, U is a velocity scale and ν is the kinematic viscosity of the fluid) was between 100-1000 implying an operating regime where both inertial and viscous effects of the fluid were important. Two different cases were considered. In the first we investigated a closed geometry, in which the fluid was air at Reynold's Number of 500-1000, and the object was a soft cylindrical shell. In the second, an open geometry was investigated, where the fluid was water at Re of 100-500 and the object a thin but stiff flat rectangle.

Fluid elastic interactions in closed geometries are especially important in biological systems examples of which include blood flow through the circulatory system [14], air flow through the pulmonary system [24], sounds created in the cardiovascular and pulmonary systems [23] and production of sound via interaction of air flow with the vocal organs. The last example is the one we were interested in, specifically in the context of song production in birds. There are over 4000 species of song birds, each with their prototypical sounds and song structures. Neurobiologists are interested in understanding the neural circuitry that underlies the learning and reproduction of complex songs. They wish to map brain activity to muscle activity in the vocal organ that ultimately leads to production of song. However the vocal organ of the bird, the syrinx, itself is a complicated organ, a hub of complex hydroelastic interactions that lead to sound production. The sounds created can be complicated and experiments show that the syrinx behaves like a low dimensional nonlinear dynamical system. This is our interest. We would like to understand the physics of the syrinx, the

process of sound production and its controllability in order to help decipher the secret language of the brain. The goal then is to provide the neurobiologists some insights into how nonlinearities in an interacting hydroelastic system can be controlled by understanding the underlying phase space of the nonlinear system. Control then amounts to specifying a path through phase space and the questions are 1)what are the dimensions of the phase space and 2) how many parameters are required to reliably sample large parts of it.

Several different avenues of research have been explored, historically, in this direction. The earliest theoretical studies consisted of simple 1-d models of the syrinx with the Bernoulli pressure ($p \sim -u^2$) of the fluid acting as the driving force [1, 2]. Under certain conditions of flow and tension in the syrinx, self sustained oscillations were observed [10]. Improvements on the earliest theories led to ones where the syrinx along with the airflow were modeled as a Van der Pol oscillator-type system, where limit cycles arose under certain conditions on the control parameters [27]. Adding mode structure to the oscillators allowed theorists to recreate some simple tonal songs of birds like the canary [30]. Meanwhile, experiments with excised syrinxes revealed that they behaved like nonlinear dynamical system when an airflow was imposed [22]. Increasing the external pressure led to transition to chaos, indicating the inherent nonlinearity in the fluid elastic interactions in the syrinx. Recently physical models [3] have been explored to attack some questions about onset of phonation in such closed systems, however the question of controlling the sounds remained relatively unanswered. We sought to understand the phenomenon of song production in the syrinx experimentally by creating a physical model of the syrinx and probing its dynamics.

The simplest model was chosen, a soft elastic tube (made out of Nitrile rubber) of diameter 2.5-5mm and length 2cm represented an approximation of the throat of a small song bird like a canary. Self sustained oscillations were observed when air flow was imposed through the tube. Moreover transitions to different phases of oscillations were observed when dynamic muscle action was mimicked using an external probe. Thus this simple model not only displayed some of the complex nonlinear features observed in excised syringes but also could be controlled dynamically. In Chapter 2 we describe the creation of artificial birdsong by dynamically controlling the path of an oscillator through its phase space.

In the open geometry we studied swimming of a small fish like device in a dense fluid like water. Most theories of fish swimming are steady. They involve considering the problem as one in which an "added" mass of water is continuously accelerated by the body and tail thus providing thrust [11]. While such mechanisms explain slow swimming velocities of fish that produce undulatory motions of their bodies to propel themselves forward, they do not explain rapid accelerations, quick turns, and fast swimming often seen in many fish. Recent PIV visualization experiments have shown that some fish create highly linked vortex rings that produce a highly directed jet that the fish uses to propel itself [9]. In a typical quick start by a bluegill sunfish, the animal curves itself into a C shape within 10ms and then directs various jets to create forward thrust [6].

The motivation then is to understand and use unsteady dynamics in the fluid to augment thrust production. Unlike fish that make a few rapid flicks of its tail to accelerate quickly to avoid predators or attack prey, insects have to continuously

generate thrust in order to balance gravitational forces. Moreover they can hover, twist and tumble through the air with amazing ease. Recent PIV studies show insects can enhance lift production estimated from steady state studies by a factor of 1-3 by creating and manipulating vortices in the fluid [28]. These studies also indicate that insects use their wings like aerofoils translating at a high angle of attack that rapidly rotate at the end of each half cycle so as to maintain a positive angle of attack throughout [18]. Some insects create a figure 8 pattern with their wings while hovering. The Reynolds number for these insects is 100-5000.

Motivated by these phenomena, we wished to design and analyze a small robotic device that used unsteady fluid effects to enhance thrust production. The length was chosen to match that of small fish and the Reynolds number matched that of insects. The idea was to augment added mass inertial forces with forces generated by vortices as seen in insects. The tail was a thin elastic cantilever that was impulsively accelerated using a magnetic coil assembly. It is known from studies of unsteady fluid dynamics that a aerofoil at a high angle of attack starting from rest can incur larger lift and drag forces that steady state values based on instantaneous values. The impulsive action of the tail was used to take advantage of this feature of the behavior in fluids. Terrestrial insects use impulsive forces by storing elastic energy over a long time scale and releasing it rapidly to travel long distances by jumping. In the second part of this thesis we studied the effect of impulsive forces generated by solid body on a fluid medium. In an inviscid theory of fluid dynamics, that is one in which the effects of viscosity are ignored, the flow around a thing airfoil can be modeled with potential flow. However at the sharp edges around the airfoil the

fluid has undergoes large accelerations, and at some length scale the effect of viscosity cannot be ignored. Potentail flow can be modified by adding net circulation to the aerofoil that compensates and cancels the singularities in the fluid velocities around the edges. This is called the Kutta Condition and mathematically gives rise to the lift force on the aerofoil. In reality the Kutta condition applies to steady state flows. No net circulation can be created in an inviscid fluid, hence the circulation around the foil must be matched by an equal and opposite amount of circulation in the fluid. The is the content of Helmholtz theorem. When the airfoil is translating steadily the circulation in the fluid (starting vortex) rolls up into a vortex and is far from the airfoil but attached to it. While starting or rapidly accelerating however the starting vortex may not have enough time to detach from the airfoil completely and hence delay the lift production. This is termed the Wagner effect. Although this effect is deleterious to lift, it may be possible to enhance lift production transiently using a leading edge vortex.

In Chapter 3 we report on the design and analysis of a fish type robotic device that uses impulsive forces to create thrust. The length of the device was 5 cm and maximum instantaneous velocities of unto 35 cm/s was observed at a hydrodynamic efficiency of about 0.3. It was observed that the flow behind the device was extremely unsteady. A ratio called the advance parameter defined as $J = u_{tail}/u_{forward}$ measures the contribution of the unsteady flows to thrust production; a J=0 corresponds to hovering and a J=∞ coresponds to gliding flight. In our system we observed J$\sim$ .5, indicating that flow unsteadiness created by the tail dominated the thrust production.. The control parameter was the frequency of the driving force. A peak in velocity was

observed at 18Hz and corresponded to the creation of two well formed jets, while for other frequencies far from 18Hz, the wake consisted of unlinked vortical structures. Moreover the interaction of the cantilever with the unsteady flow modified its own oscillatory pattern. For a linear damped system, we expect the power spectrum of the amplitude of oscllation as a function of drive frequency to display a Lorentzian behavior. However for our device we found this to be the case only close to the resonance frequency of the first mode of the cantilever. Far away from resonance a new mode arose in which the tail tip displayed a figure 8 pattern, in a manner very similar to that used by some hovering insects. The coupled hydroelastic system therefore behaved like a nonlinear dynamical system driven by the magnetic coils that exhibited different modalities of oscillation depending on the control parameter, the drive frequency.

The unifying theme of the thesis was understanding the complex interaction that arises between a fluid and an elastic object in simple physical systems. The interaction leads to behavior of the entire system that can abstracted as a nonlinear dynamical system displaying patterns that change based on some effective control parameters. These different behaviors, remarkably, capture aspects of some natural phenomena and can be used as first order models or to build a device mimicking a process observed in nature. In this thesis we studied two such phenomena, singing in small birds and swimming of a small fish like robotic device.

Chapter 2

Bird Song: In Vitro, In silco

2.1 Introduction

Bird song has interested humans since ancient times, and still serves to inspire artists and scientists from a range of fields in understanding its evolutionary origins, ecological significance, neural correlates, and biophysical mechanisms. Here, we focus on this last question from the perspective of building a controllable device inspired by the avian syrinx that allows us to mimic simple auditory gestures, and a minimal mathematical model of the system that poses the problem of song mimicry as one of optimal tracking and control.

Much about the physical mechanisms that allow birds to produce songs with rich harmonic content is still unknown. The avian syrinx located at the intersection of bronchus and trachea, is a complex physical system where air flow couples with an elastic membrane to produce sounds and when actively controlled by muscles, song. Previous studies have localized some of the mechanisms of vibration via in-vivo imag-

ing, physical modeling and computational approaches. However, many unanswered questions remain about a minimal system with enough freedom to reproduce birdsong. In this study we describe a biologically inspired physical model where some aspects of musculature has been incorporated allowing us to mimic a range of songs within a certain species and also move between species by changing material and control parameters.

The enigma of bird song has attracted functional biologists, neuroscientists, mathematicians, physicists and acousticians. Various kinds of attempts have been made to understand the complex sound generating organ, the syrinx. The modes of research, historically and categorically , have been threefold, theoretical or computational models [10], [27], [30] , visualizations in intact or excised syrinx [16], and physical models [3]. These efforts have uncovered some of the mysteries; the sound generating area has been localized to medial and lateral labia [17] and numerical computation of coupled oscillator models have captured some aspects of phonation (onset of sound production, and nonlinear phenomenon such as period doubling or onset of chaos).

The syrinx is the area where the bronchus meets the laryngeal cavity. Endoscopic imaging [16] of preparatory stage of phonation shows a rostrad movement of the of the entire vocal organ by the action of muscles, that also stretch the elastic tissue thereby applying tension. At the same time two fleshy masses, the medial and lateral labia, situated in the bronchus slightly behind the opening, are drawn in forming a valve. Air pushed through these labia, via the action of the lungs, sets them into self sustained oscillations creating song. Simultaneous monitoring of muscle activity around the syrinx, showed strong correlation with the frequency of sound produced.

The first serious functional model of the avian syrinx was presented by Greenewalt [12] in 1969 and later elaborated by Brackenbury [1] in 1979. Brackenbury suggested a flutter like mechanism gave rise to the sounds created (the birds being studied were fowls).The physics was described by a simple linear model $m\ddot{x}+\beta\dot{x}+[K(x)-F(U)]x = 0$, where m,$\beta$ and K(x) were the apparent mass (including added mass from the air), damping and stiffness of the membrane and $F(U) \sim U^2$ was the aerodynamic force exerted by the fluid moving at velocity U. They conjectured that the onset of phonation occurred via a flutter instability when the apparent stiffness $K(x) - F(U)$ was negative and derived $U_c = \sqrt{K(x)/F(U)}$, the critical flow speed for phonation. The first models though simple captured some physics but were far from complete. Fletcher [10], elaborated these theories by indicating the vital importance of the nonlinear coupling between the fluid and elastic response of the syrinx. This coupling allowed phonation to explained as a self sustained oscillation mechanism. Further, the strong nonlinearities lead to mode coupling between different modes (not necessarily harmonics) of the elastic membrane giving rise to complex but repeatable sounds. These models did not try to capture any elements of control of the song produced, but answered some questions about onset of phonation and creation of complex sounds. Following the work done on human vocal folds, computational models were developed by Mindlin et at [30] to address the question of control. By modeling transverse and lateral waves on the syrinx and changing physical parameters like the Bronchial Pressure and Labial Tension, it was shown that certain syllables could be reproduced. Such simple gestures are characteristic of songs produced by song birds such as the canary, whose songs are mostly single frequency.

Most birdsongs are however not single frequency, songs produced by the Zebra Finch contain both large harmonic and chaotic content, with rapid transitions between the two, and nonlinear dynamics such as period doubling and mode locking transitions . In a set of experiments performed by Fee[22] it was demonstrated that an excised syrinx behaved like a low dimensional nonlinear dynamical system. Sound was produced when pressure was applied across an excised syrinx, and showed a harmonic spectrum. When the pressure was increased above a critical the sound transitioned from periodic to aperiodic behavior. Hence unlike a human vocal organ, the shape of the sound produced is controlled by the intrinsic nonlinear interactions between the fluid and the syrinx, and not by the filtering action of the throat and beak.

Motivated by these observations we seek to find a minimal physical system that can explain and reproduce the phenomenon of song creation by the avian vocal tract. The vocal system of the bird consists of lungs that control the flow rate or pressure, the syrinx which oscillates to produce the sound, muscles that control the syrinx and filters formed by the beak and tongue. In our system we modeled the lungs with a constant flow source, the bronchus with the syrinx at its mouth, by a thin cylindrical elastic tube, and the action of the muscles by a linear motor that pressed down on the cylindrical tube mimicking a squeezing action by the muscles (fig [1a] shows a schematic of the syrinx and [1b] shows the corresponding physical model). We chose to ignore the acoustic filter even though it might have a considerable effect on the sound generation, because we wished to isolate the intrinsic nonlinear dynamics of harmonic sound production by the artificial syrinx. The first goal of the present study was to investigate the role of nonlinear dynamics in sound production by the artificial

syrinx under static and dynamic action of the linear motor. Briefly, we found that the cylindrical tube sustained single frequency, multi frequency and chaotic oscillations under static probe action and displayed many other nonlinear phenomenon like period doubling, transitions in and out of chaos when probed dynamically. The second goal was to address the problem of control by creating song by varying the dynamical parameters in the problem, which in our case turned out to be dominated by the position and acceleration of the linear motor. A way to phrase this question is to ask whether it is possible to think of a bird song as an abstract "path" followed by a nonlinear dynamical system as its physical parameters are varied (on a time scale much shorter than the intrinsic time scales of the system).

The dimensions and material of the cylindrical tube were chosen to be close to that of small song birds like finches and canaries. It was observed that the length of the tube did not play a crucial role in determining the structure of the sound produced. The final material parameters were length 2cm, diameter 2.5mm (although devices with d=3-5 mm were also measured), thickness .1mm, Young's Modulus 2MPa and a bending frequency $\omega_b \sim \sqrt{\frac{E}{\rho}}\frac{h}{L^2} \sim 1kHz$. The device was created by attaching two pieces of nitrile rubber (2cm x 2cm) with a rectangular section (2.5mm x 2cm) in the middle left vacant to form the vocal tract (Figure[1b]); with flow imposed, the device assumed a cylindrical shape.

The device was open to the atmosphere at one end and fed with air from the other, controlled by an Alicat Scientific flow meter. Translation stages (T_x,T_y) attached to the rear end longitudinally and at the open end transversally were used to apply strains on the device (see schematic Figure[1b), which were measured by the strain

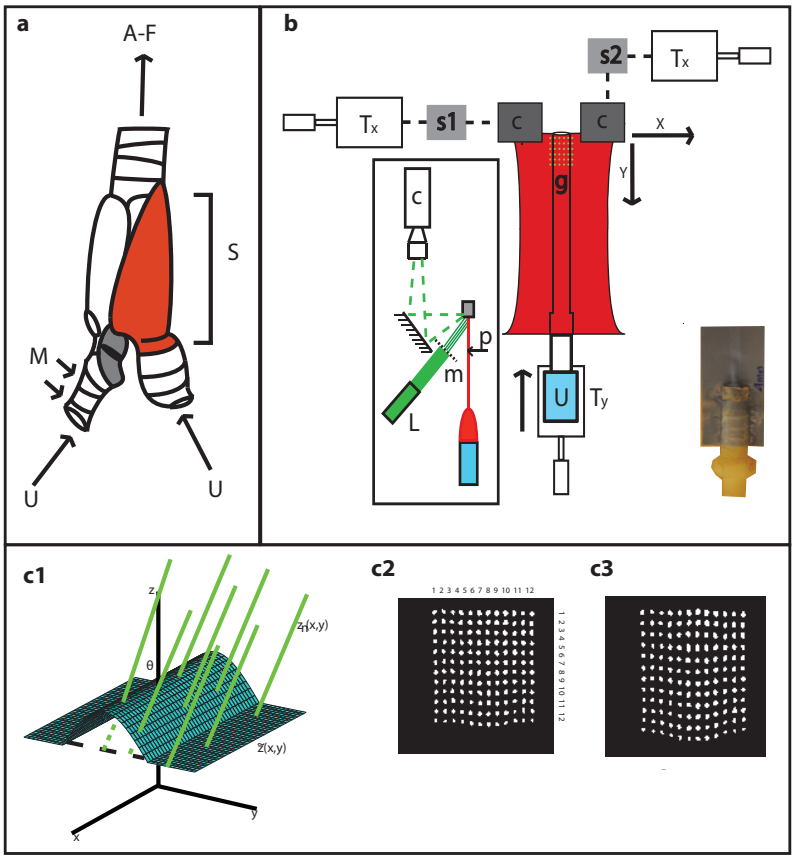

Figure 2.1: (a) Schematic of a zebra finch vocal tract. S is the sound box (syrinx) of the bird, U is airflow coming from the lungs, A-F is the acoustic filter formed by the beak and trachea, M denotes muscular action along the length of the bronchus. (b) Schematic of experimental setup. c1,c2 - clamps; s1 - strain gauge to measure lateral tension; s2 - measure longitudinal tension ; Tx - translation stage to change lateral tension; Ty - stage changes longitudinal tension; F - flow meter; g - grid projected onto device. Inset shows side view of the setup. L - 10 mW Green laser pointer; m - mask used to produce grid; p - probe used to excite device; c - High speed video camera (upto 90kHz frame rate). The probe p is a linear motor that can be used to excite the membrane by pushing anywhere along its length. An image of the actual device is shown in the bottom right corner.(c1-3) Demonstration of the principle of the optical reconstruction. c1) shows the top surface of the device, described by the function z(x,y), being impinged by pencils of laser light described by the functions $f_n(x, y)$ where n is a label. The light is incident on the device at an angle θ and the dashed lines show the intended path of the laser before it is intercepted by the surface. c2 and c3 show images of the raw data with the flow turned off and on respectively. The distance that each point in c3 has moved from its original location in c2 is proportional to the height at the observed point and this information can be used to reconstruct the entire surface in three dimensions.

gauges S1 and S2. These stages were not actuated dynamically but were used to set the pre strains on the device which determined a "starting point" in the phase space of the dynamical system. In addition muscle action around the syrinx was simulated by the linear motor that pressed down transversally (perpendicular to the plane of the device) along the tube (P in fig[1b, inset]). The control parameters were tensions in the lateral and longitudinal direction $T_x, T_y \sim .1-1N$, streching frequency $\omega_T \sim \sqrt{\frac{T}{\rho}}\frac{1}{L} \sim 1kHz$, flow rate, $U \sim 5-10m/s$ displacement of the linear motor into the membrane surface, $d \sim .1-1mm$ and the Reynolds number $Re = \frac{UL}{\nu} \sim 10^4 - 10^5$

We wished to improve on earlier attempts that reduce the song to a definite path in abstract phase space [30], but do not convert this information into relevant physical mechanisms. Recently Elemans et al,[3] demonstrated sound producing sustained oscillations in a different geometry than ours. However one limitation of this physical system was the absence of control which we tried to incorporate into our model.

2.2 Measurement Techniques

The main experimental technique used in this study was three dimensional imaging of the device to explore the different regimes of oscillations. The space and time resolution required ($100\mu m$,$100kHz$) rendered normally stereoscopic imaging too cumbersome to implement. Instead an optical square grid of 144 points was projected onto the device by passing an expanded beam from a laser source through an appropriate grid. The laser struck the device surface at 30 degrees from the normal (see figure[1c]). For a flat surface, this grid of points appeared in a rectangular configuration, but any curvature deformed the grid; tracking this deformation allowed

reconstruction of the height profile of the entire surface. The caveat was in plane motion could not be tracked, since only out of plane motion of the device causes the grid to deform. In our case out of plane motion was dominant and this imaging technique could capture three dimensional motion to a high degree of accuracy. Another advantage of this technique was that it only required a single camera for 3-d imaging.

The optical source was a 10mW laser pointer (from Dragon Lasers), which was beam expanded to 4 times using a 4:1 telescopic setup. The expanded beam then passed through a grid (7mm x 7mm; 12 holes on each side), made out of laminated paper, in which holes (d=.25 mm; spacing .625mm) were cut out using a Versalaser laser cutter. The grid was placed no more than 5cm away from the device to prevent any diffraction rings, from the holes, from interfering with the imaging. The images of the grid projected onto the surface of the membrane were captured with a Phantom V7.3 high speed camera at 88kHz frame rate.

The laser beam was collimated so that the size of the grid projected onto the device was 1:1. The grid created thin pencils of laser light that (Figure[1c]) traveled along a plane parallel to the y axis, and were labelled $z_n(x) = mx + c_n$, where n=1...144 and $tan^{-1}m$ was the angle the laser made with the device and c_n parameterized the z-intercept for the different pencils. The surface being imaged is some function $\tilde{z}(x, y)$; therefore the bright spots on the camera indicate the intersection of $z_n(x)$ and $\tilde{z}(x, y)$, x_n . The height at x_n can be derived using the relation $z(x_n, y) = mx_n + c_n$, where c_n/m is x position of the points on a flat surface. Thus by measuring the intersection point we get information about the height. This trick allowed us to only use 1 camera saving a huge amount of extra effort. Our imagining gives us the

position and height at each of the points the laser intersects the surface. In our setup we have 144 pencils of light (12x12 square array), and we spline between these points to recreate a continuous surface. In essence we are spatially sampling the surface for which, Nyquist's sampling theorem, states that minimum resolution is twice the sampling frequency which in our case is 0.4mm. Since the dominant length scale is the diameter (2.5mm) no problems with under sampling were expected.

Sound was recorded using a Senheiser 825-S microphone, preamplified using a Behringer Tube Ultragain Mic 200 and recorded at 44kHz via the computer sound card. Images were recorded by Phantom V7.3 at 88kHz. The spatial resolution of the measurement was .1mm. The major source of noise was due intensity and mode fluctuations in laser.

2.3 Experiments and Results

In this section we describe the dynamic and acoustic response of our device. The information that we get from our setup is the 3d reconstructed surface of a portion of the device recorded at 88kHz, and the sound waveform recorded at 44kHz. First we describe results where there was no probe present, and the parameters under control were the two tensions T_x and T_y, and the air flow rate, U. The experimental protocol was to first set the tensions and then to increase the flow rate in steps of .1m/s waiting 2 s at each step from 0 to 5m/s. Figure[2a] shows a plot of the Intensity of sound produced as function of these parameters with T_y=0.11N. The sound Intensity shown is from the step when the flow velocity was increased. The observation was that the qualitative dynamics of this system did not depend sensitively on T_y for strains less

than 0.5 (this was the regime of operation for the set of experiments described). From the data presented we found the critical velocity for onset of sound (in the scenario where we first set T_x and swept U) was inversely related to the applied tension,T_x. This qualitative behavior was shown by devices of different radii also.

The sound intensity increased approximately linearly in this regime, but for large values of U the sound saturated since the membrane stiffens for large deformations. Figure[2b] shows the fundamental frequency of the sound produced as a function of U, the different lines correspond to different values of σ (the green and magenta ones correspond to the positions indicated in Fig[2a]). The frequency showed weak linear dependence on U and T_x, and in order to reproduce the large frequency range of a song bird, unreasonable large strains would be required (roughly a factor of 6). Experimental evidence shows that birds do not incur such large strains while phonating. Hence the device as operated would not be able to reproduce the complex songs of song birds.

Although the set of experiments just described show that sound can be produced by applying tension at the mouth of the device, it would be difficult to make it sing like a bird. Results show that the frequency depended only weakly on the applied tension and the flow velocity. So such a model for a birds syrinx would not work because it is not possible to produce sounds with large frequency range as commonly seen in birds. Fee in his paper on measurements [8] of the properties of the syrinx made a similar claim. His elastic measurements on a zebra finch syrinx showed that no more that an a factor 2 increase in spring constant, not the factor of 50 that would be required to explain the factor of 7 frequency range of a zebra finch from a lumped

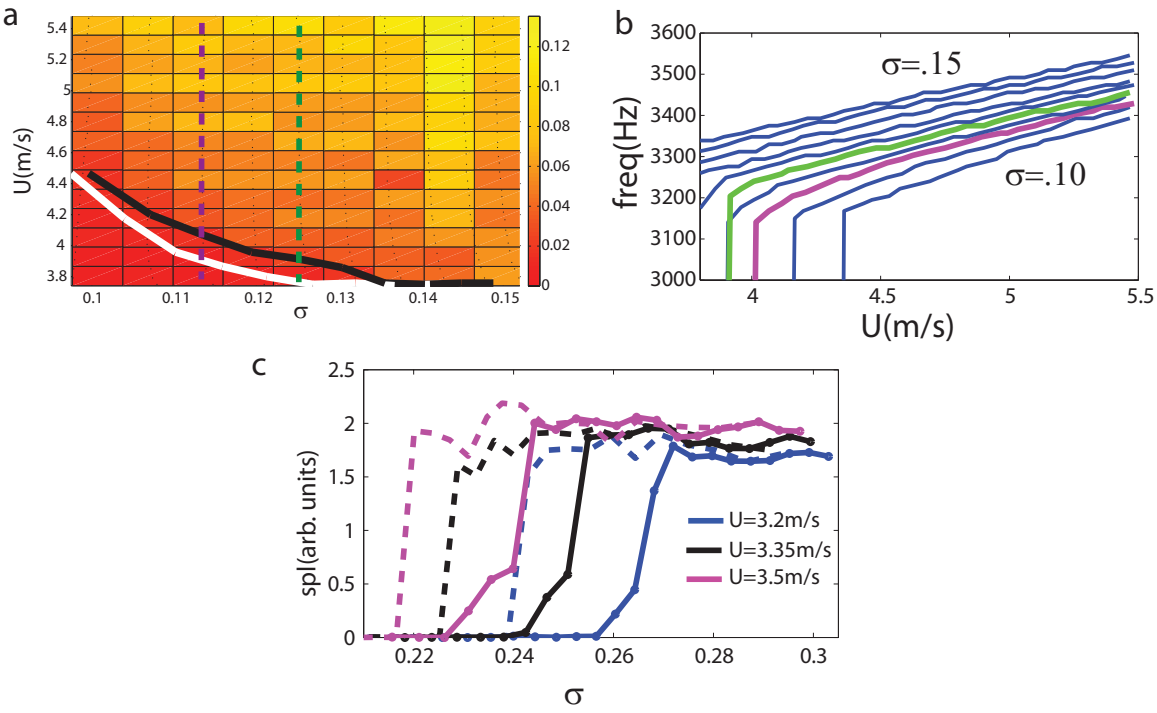

Figure 2.2: a)Intensity (in arb. units) as a function of T_x and U with T_y fixed at 0.11N. $\sigma = T_x/wtE$ where w and t refer to the width and thickness of the portion under stress. The dots in the figure show the points at which data was collected. In the experiment T_x was held constant while the flow velocity was increased in steps of .1m/s. Then T_x was changed to a new value and the experiment was reiterated. The black line indicates start of phonation white line indicates its end. (b) shows the fundamental frequency of the sound produced as a function of velocity for the range of σ .1-.15. The frequency only changes by a factor of 1.1 for a change of 1.5 in σ indicating that this mode is not suitable for producing large frequency changes as seen in real bird songs.(c) shows rms intensity of sound produced as a function of large values of σ for three different flow velocities. As σ is increased past the ranges indicated in (a) phonation first stops and ensues again at larger values of σ. Large hysteresis is observed as shown in the figure.

spring model.

When the linear motor presses down along the length of the device, it also undergoes self sustained oscillations and produces sound, once the motor has pressed past a critical depth. The precise value of the critical depth depends on the applied pre tensions and the flow velocity. The frequency structure of the sound produced depends on the prestrains applied to the system, flow velocity, probe depth (along the z axis) and position along the length of the device However, for a fixed y position (see Figure[1b] for coordinate system) of the probe and flow velocity, the sound could be turned on or off and its frequency structure changed with its z position(depth). The instability at the onset of sound production was observed to be either super or subcritical depending on the precise value of the control parameters. The physics of the system can be described as that of an excitable system with z-position of the probe serving as the control.

We found that the pressed tube can either be quiescent or have three kinds of oscillations. Figure[3] shows the rough landscape of the phase space of this device as a function of flow velocity and z position of the probe. These results are for a fixed y position of the probe (.5 cm from the mouth) and pre strains(.2 in both directions). The different colors correspond to the different phases. The experiment was performed by first fixing a flow velocity and then pressing the probe down in steps of 0.1mm. The sounds were characterized based on their frequency structure. If there was one dominant frequency the sound was characterized as tonal (red), if the sound had a multi harmonic structure with almost equal energies in a few harmonics then it was characterized as solitary (blue) and chaotic if multitude of

peaks were observed in the spectrum with no obvious relation between the frequencies. Finally there was a seldom seem regime where the spectrum had a multi harmonic structure embedded in a chaotic background. This is an intermittent regime which we characterized as a mixed phase (black). In the first kind(red), the tube surface undergoes sinusoidal variations and produces a near single frequency sound. There are often higher harmonics present with very little energies compared to the fundamental. These only distort the shape of the waveform but do not produce a different "phase". The second phase (blue) was qualitatively different, solitary bumps (the size of the bump is about that of the diameter of the tube) form at the location of the linear motor and consequently travel to mouth. Following a longer recovery period this solitary motion is repeated. In this case the sound produced had high harmonic content. Transition from the tonal to solitary regime mostly happened rapidly within a couple of cycles, but sometimes it happened through a period doubling transition For certain values of transverse tension at the mouth these two modes coupled with each other to produce a sound with high harmonic density. An example of this kind of mode will be discussed later, since these modes were necessary to reproduce a zebra finch song. The chaotic regime (green) encompassed two kinds of behavior, one in which the timing between consecutive pulses was chaotic and the other where the solutions jumped chaotically between solitary and sinusoidal phases.

The structure of the phase space depicted is not the only possible. For example for different pre strain values or different y-positions of the probe we found regions where only tonal or only solitary sounds were produced. If the probe was placed farthest from the mouth then the sound produced was only chaotic and no sinusoidal

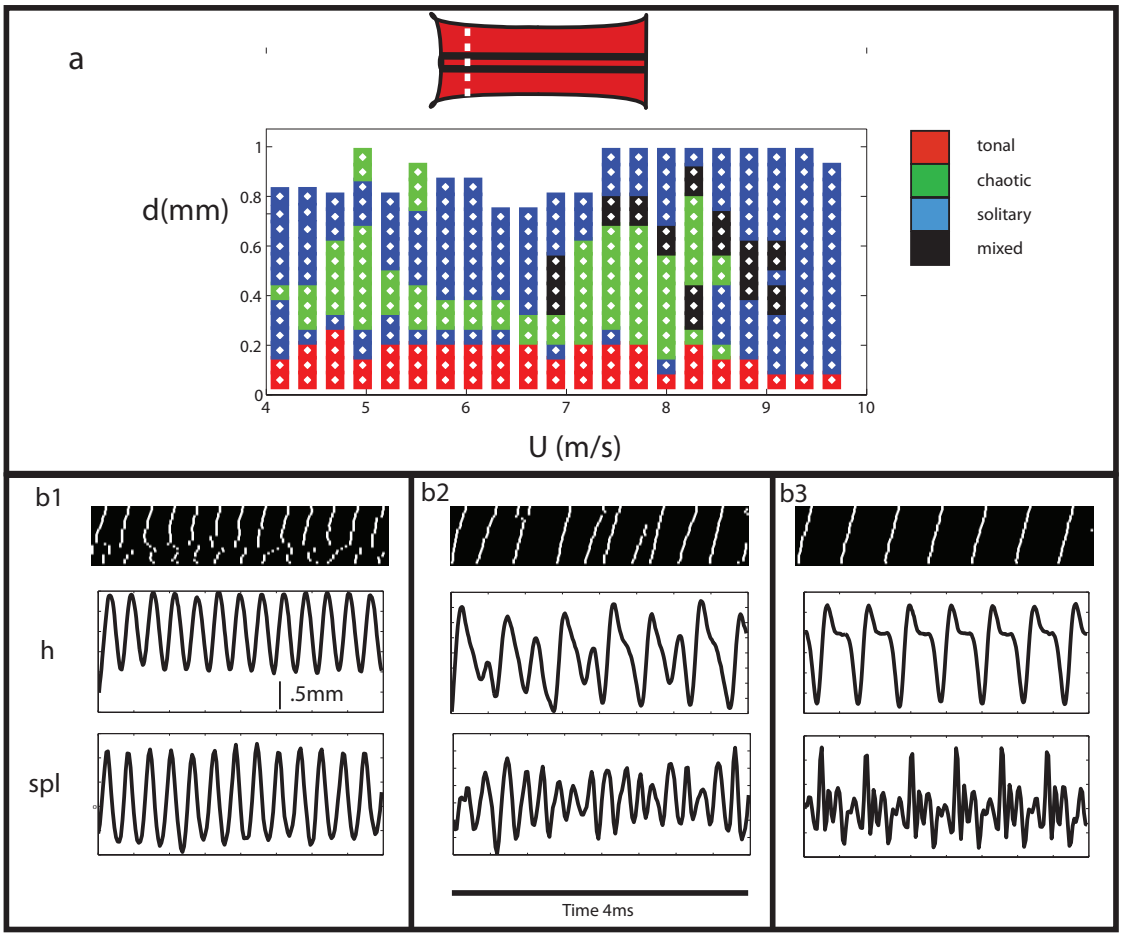

Figure 2.3: (a) shows the phase space of a device with diameter 3.5mm sx = sy = .2. as a function of flow velocity (U) and probe depth (d) measured relative to the first depth at which sound is produced. Note that the solitary regime may have further subharmonic bifurcations A "mixed" phase between chaotic and solitary also exists, marked in black in the phase space . (b) Digitized Kymograph, height (h) of the membrane at x=w/2 and y=.5cm from the mouth, (white dashed line on the device schematic) and sound pressure level (spl) for the three regimes, tonal, aperiodic and solitary.

or solitary phases arose. Hence the phase portrait shown in the figure[3] can be thought of a section through a higher dimensional phase space.

The sinusoidal regime occurs normally when perturbations to the surface are small, and the device is being pressed close to the mouth. As the probe is moved further away from the mouth and towards the end, this mode (regime) cannot be excited anymore. However along an intermediate distance along the tube we can still observe traveling sinusoidal waves as shown in Figure[4a, where one period of oscillation is shown]. Pushing further down ($\sim$0.1mm) causes a period multiplying bifurcation as shown in Figure[4b]. Figure[4b] shows a similar 3d reconstruction of the device and Figure[4c] shows the height of the membrane at different points along the length of the tube (see figure to see exactly where) as a function of time. We found that the cycle started with a traveling sinusoidal wave of the kind described above (0-0.17ms, denoted by the bump A in figure[4c]). Immediately after this passed, a larger depression was created and traveled to the mouth(.239ms-.375ms, denoted by the bump B in figure[4c]), after which there was a rest period (not shown in 3d reconstruction) and the cycle repeated. The labels A and B in Figure[4c] indicate these traveling waves. Note that the sinusoidal wave does not travel all the way to the mouth. The second depression is still not completely of the solitary kind. To get into the solitary phase we had to press down 0.1mm further into the device.

The reconstructed solitary phase is shown in Figure[5c]. At 0.04ms we see the depression start to form. At about 0.1ms the depression has completely formed and starts to stray away from its point of origin. The depression travels to the mouth of the device and there is a rest period after which the cycle repeats. The sound

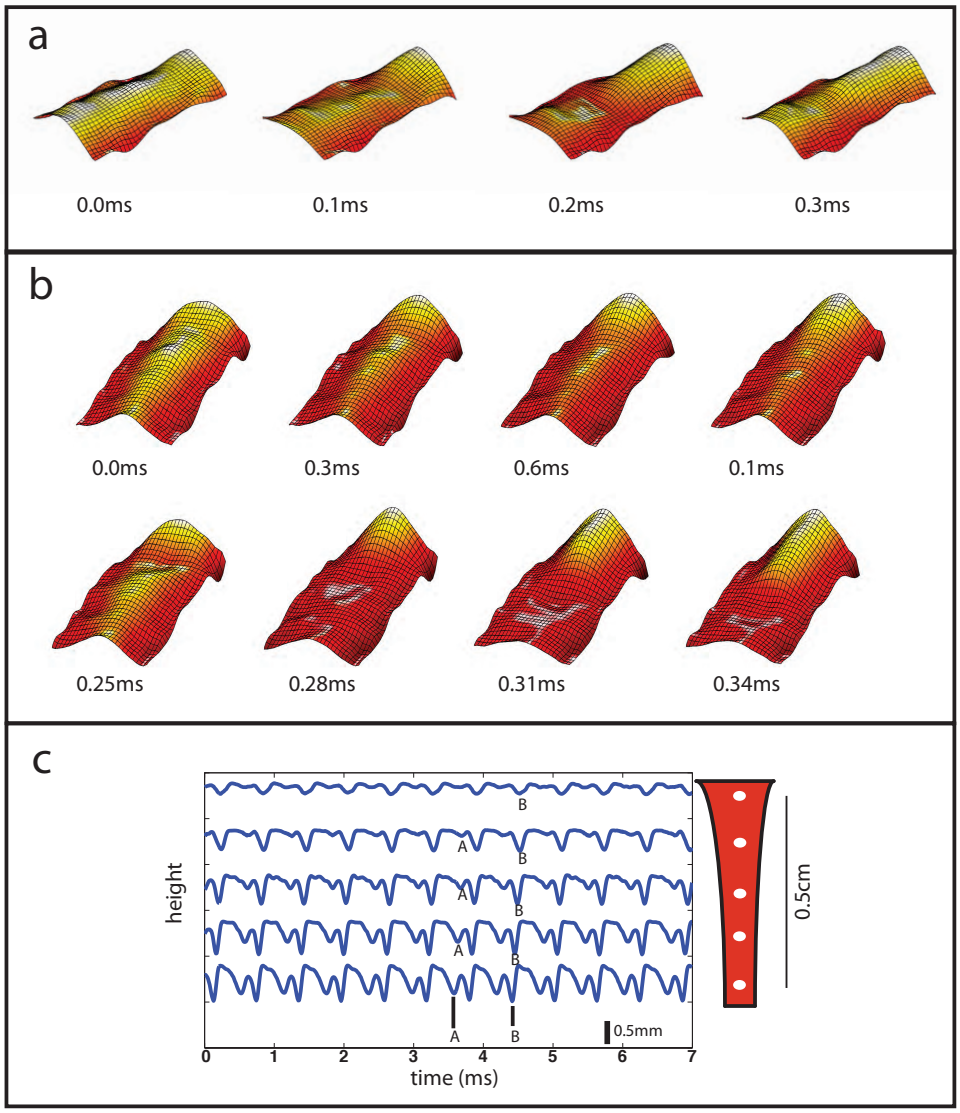

Figure 2.4: (a) shows the 3d reconstructed image of the tonal mode of vibration. In this case the probe was placed 0.5cm away from the mouth, and the tonal mode appeared as gentle undulations of the surface of the tube. (b) Period doubled mode- This mode shows a lower fundamental frequency that than the corresponding tonal mode (not shown, the original tonal mode had time period 0.2ms), that arises because a shallow solitary solitary wave (0.25-0.34ms) is created right after a sinusoidal variation has passed, thereby extending the total period of the mode. (c) Shows a time trace of the height of the device at different points along its length, delineated by the white dots of the sketch of the device (to the right of the plot). The sinusoidal variation is shown by the bump at A and the solitary pulse is shown in B. Note that in order to see this mode one had to press the motor 1cm from the mouth. As a result the tonal mode did not make it all the way to the mouth.

produced in this case had large harmonic content. Figure[5b] shows the dependence of the fundamental frequency on the z-position of the probe. The frequency shows a strong linear dependence on the probe position. The strain incurred at the position of the linear motor is $\sim \sqrt{1+(z/r)^2}-21 \sim (z/r)^2 << 1$ (where r, the radius of the tube sets the length scale of the depression formed by the linear motor). For this phase it is possible to get a large change in frequency by applying a small change in strain values. There are two time scales associated with this mode. The first is determined by the wave speed of the solitary bump and the second is determined by the recycling time of the solitary wave. The wave speed was measured by thresholding the reconstructed 3-d images based on the height profile (see figure[5a]). The thresholding was set to identify the solitary bump as it traveled across the tube; and by extracting the midline of the thresholded image and placing consecutive images contiguously a continuous image was formed, where the history of the solitary pulse showed up as a connected line (see kymographs in fig[3b]). We found within the accuracy of our measurement that the bump traveled at the same speed throughout its entire course at roughly 25-40m/s.

Static pressure measurements on elastic cylindrical membranes [25] show that the cross-sectional area is a single valued function of the transmural pressure ($p_{external} - p$). However the slope $\frac{d(p_e-p)}{dA}$ is not constant; the cylinder is stiffer when the cross-sectional area is large, but becomes softer as the area becomes small, till it finally buckles. Dynamically, the amplitude of the oscillations have to large enough so the the device can locally buckle and cause the separation of time scales. To predict these effects we need to solve the elasticity equations and use the Navier Stokes equations

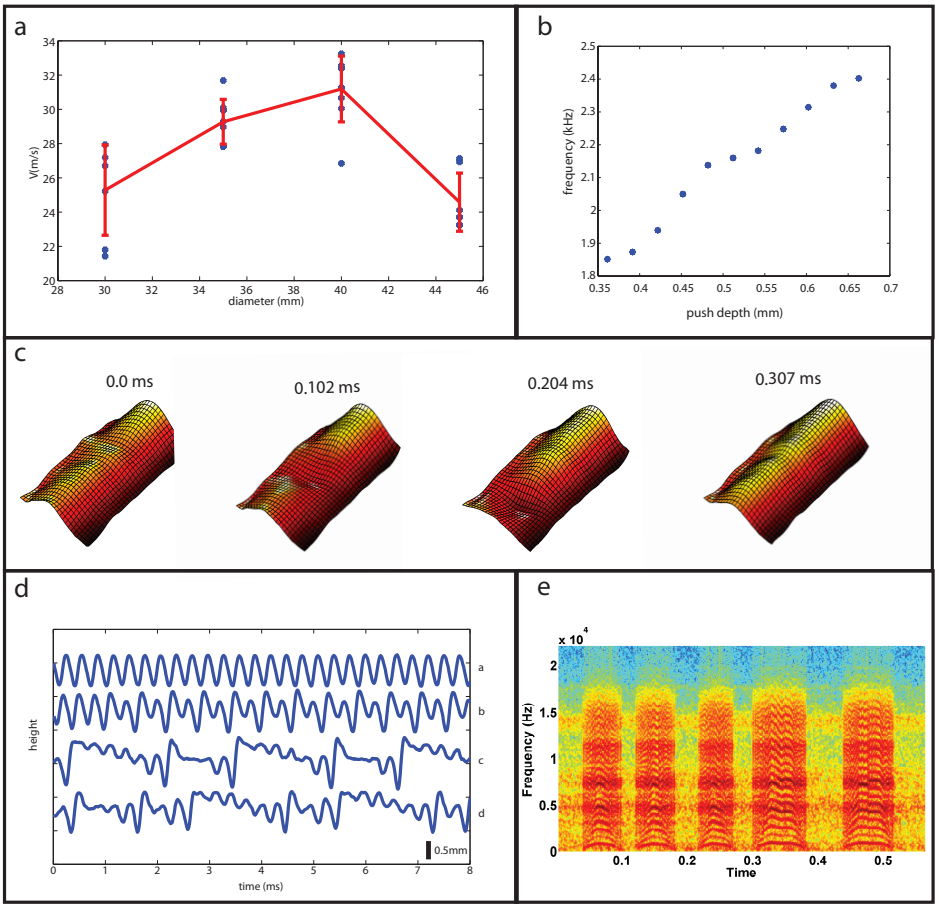

Figure 2.5: (a) Wave speed of the solitary mode as a function of radius of device. For each radius flow velocity and push depth was changed to generate the data points. The speed is measured by first extracting the midline from reconstructed 3d image from each time frame and place next to each other to create a kymograph. The kymograph is the digitized and the solitary wave shows up as a straight line. The slope of this line gives the wave speed. (b) Fundamental frequency of the solitary mode as a function of push depth. The frequency changes by a factor of 1.5 when push depth is changed by a factor of 2. This range is further increased when the sound is dynamically created. (c) 3d reconstructed images of the solitary mode. A solitary bump is created close to the probe position (below the surface being imaged)which then travels to the mouth. After the wave passes there is waiting period after which another pulse is created. The frequency is controlled by changing the time interval of the waiting period. (d)Shows height at one point on the surface as a function of time for different push depths (increasing from a-d). In a) sinusoidal mode is observed, b) a period doubled mode c)-d) higher period mode created by interaction between the solitary mode and tension modes at the mouth of the device. The sound created by this mode is rich in harmonic content and some sample sounds are shown in the spectrogram in (e).

to compute the forces exerted by the flow on the membrane. For now we shall simplify this model by first looking at a 1-d model to identify the time scales in the problem.

$$\underbrace{\rho h_{tt}}_{\text{mem inertia}} + \underbrace{B h_{xxxx}}_{\text{Bending}} + \underbrace{T h_{xx}}_{\text{Tension}} = \underbrace{\rho_f U^2 h_x + \rho_f h_t}_{\text{fluid inertia}} \tag{2.1}$$

First let us compare the inertia and tension term, we find $\omega \sim \frac{1}{R}\sqrt{T/\rho_s e}$. We find a tension dependence on the frequency when we have no probe present. But in most cases the tension term is small enough that we can ignore it. The second time scale comes from comparing inertia to bending. We find $\omega \sim \frac{1}{R^2}\sqrt{Ee^2/\rho_s}$. Taking $E \sim 10^8$ we find that $\omega \sim 10^4$. This value is close to what we find in experiment, but there is another time scale, corresponding to the time taken for the solitary waves to propagate$\sim \omega r \sim 100 m/s$. This is roughly on the order of the measured wave speed of 25-40m/s. Hence this evidence suggest that the solitary waves are nonlinear bending waves on the surface of the tube, where the speed is set by the Bending modulus of the material used.

Interestingly the wave speed showed only weak dependence on parameters like applied pre tension, flow speed, radius (see fig [5a]) or z-postion of the probe. Hence it could explain the large changes in frequency observed in the device for small applied strains. What set of the frequency of the sound created was time of the rest period. The z-position of the probe, when the device is operating in the solitary mode, effectively controls the recycling time of the pulses. As mentioned before the strain at the point of contact is $\sim (z/r)^2$, where z is probe depth and r is the radius of the tube. A frequency associated with this would scale as $\sim \sqrt{E\sigma}$ where E is the Youngs Modulus and σ is the strain. Inserting the approximation for σ shows that $\omega \sim z$. Hence the local strain induced at the depression can give an explanation for the linear depen-

dence of the frequency with probe depth. The probe locally stretches the membrane, and the applied tension allows the device to undergo oscillations. However when the amplitude becomes large, the device locally buckles and couples to solitary bending waves that travel to the mouth and the cycle repeats after a rest period.

We discovered that by dynamically probing the device it was possible to turn on the different modes explained above and also control the frequency, with the z-position of the probe as control. Using these modes it was possible to mimic simple songs across many song bird species. However the song of the zebra finch shows a much higher density of harmonics, and could be not reproduced with the three modes mentioned. Another mode of oscillation that was essential to mimicking songs of a zebra finch (Figure[5d]) came from coupling of the solitary waves to tension modes at the mouth of the device (these tension modes are similar to the modes displayed as a static response to the airflow without any probe). Figure[5d] shows the height of the device 0.5cm from the mouth and a,b,c,d correspond to various z-positions of the probe in increasing order. For small perturbations sinusoidal waves occured, but when probe depth was increased (position b in Fig[5d]), a mode appeared where a solitary wave first traveled to the mouth followed by oscillations at the lip of the device. The vibrations that occured of the mouth were much higher frequency than the solitary wave and appeared when the amplitude of the bump was large. This suggests that perhaps a mode locking mechanism gave rise to this mode of oscillation. Fig[5e] is a spectrogram of the sound produced by this mode and shows the dense harmonic structure that is characteristic of a zebra finch song motif. The existence of this mode was also visually verified by simultaneous imaging both the mouth of the cylindrical

and the surface (which was painted with reflective silver paint and the imaging was done with white light).

2.4 Dynamic Control

Having established our first goal to get a qualitative understanding of the physics we now turn to the second goal, to create song. This means to dynamically control the device by guiding it through an appropriate path in phase space. The method is to program the linear motor to produces "pulses" of motion, and the shape of these pulses then determine to a large extent the spectrum of sound produced. We find that it was sufficient to keep the flow rate, pretensions, and x-position of the probe constant while pulsing the motor to achieve a reliable enough reproduction. The word reliable is a dicey one to use in this case because it was difficult to find a correct metric to characterize similarity of the original with the reproduction and visual (by comparing spectrograms) and auditory similarities were used to judge the reliability of the production. In gist, pressing the device close to the mouth produced mostly tonal sounds, pressing the middle produces solitary pulses, and pressing towards the end creates chaotic pulses. There are also subtleties involving sweeps, temporary transitions to chaos, period multiplication, which we also qualitatively demonstrate.

Figure[6a1] shows a simple song in which the "notes" are pressed and held down for 350ms. Fig[6a2] shows the position and velocity of the linear probe in relation to the sound produced. The frequency was controlled by the position of the probe. Fig[6b] shows the spectrogram and motor position of series of rapid pulses created by programming a dynamic pulse sequence to the motor. Comparison of the spectrogram

with the probe position clearly shows a transition to a period doubled sound for probe depths greater than .5mm (the white arrows indicate the region of non period doubled sound). Period doubled modes were excited in static probe measurements, but now they arise under dynamic action of the probe. Another feature from the spectrogram is asymmetry in the slope of the individual chirps. The frequency decays faster than the rate at which it increases, even though there is no obvious asymmetry in the motor position. Moreover, higher harmonics decay faster.

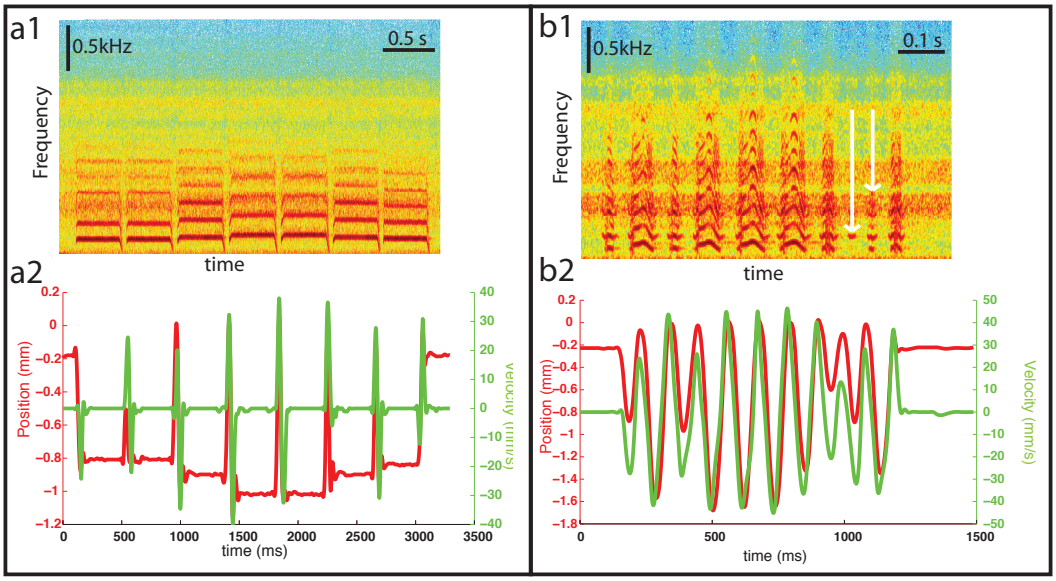

Figure 2.6: Simple Songs (a1) shows the the spectrogram of a simple song that was created by pressing down and holding a note for 0.35ms and (a2) shows the corresponding pulse sequence (red, position of the probe and green, velocity of the probe) used to program the song. (b1-2) shows the spectrogram and programmed pulse sequence for a series of rapid pulses with high harmonic content. A transition to non-period doubled sound occurs when the probe position is less than 0.5mm (shown by the white arrows)

Two complicated sounds that can be dynamically created are shown in fig[7]. The first shows a multi sweep,where the frequency undergoes a sharp modulation.

Some birds can produce a number of these sweeps in one go, a testament to their marvelous and precise control. Our device failed to capture all the oscillations in all the harmonics. Some of the higher harmonics seemed to "stall" on the downward sweeps. This might be because our excitation scheme was not symmetric in that we pushed down on the device on the upsweep but did not pull down on the device on the down sweep. Hence it is possible that the point of contact detaches and causes the device to vibrate transiently till contact is made again in the upsweep of the subsequent cycle. On the other hand the asymmetry in the spectrogram might be caused by inherent nonlinearities in the hydro elastic dynamics of the device.

The second sound (figure [7b])shows transition to chaos.To create this sound the probe was progressive pressed down in steps of .3mm, waiting 10ms at every step. The device was operated at very high acceleration rate of 25000 mm/s^2 and deceleration rate of 15000 mm/s^2. Phonation commenced with an almost pure tone sound (the higher harmonics decay rapidly in amplitude and only alter the shape of the waveform slightly from being purely sinusoidal), followed by a period doubling transition, then to chaos and finally to nearly tonal sounds again. The waveform for the first three of these sounds is shown in the panels (c1,c2,c3). The short black lines in figure[7b] indicate the position of these waveforms relative to the entire sound segment. If for a moment we imagine that these set of experiments shed some light on actual bird song production, then it shows that even with very simple control it is possible to produce very complicated sounds. The key is to find the appropriate region in phase space and then plot an appropriate trajectory through it. For example to produce a transition to chaos as with zebra finch songs, the device was biased at the boundary

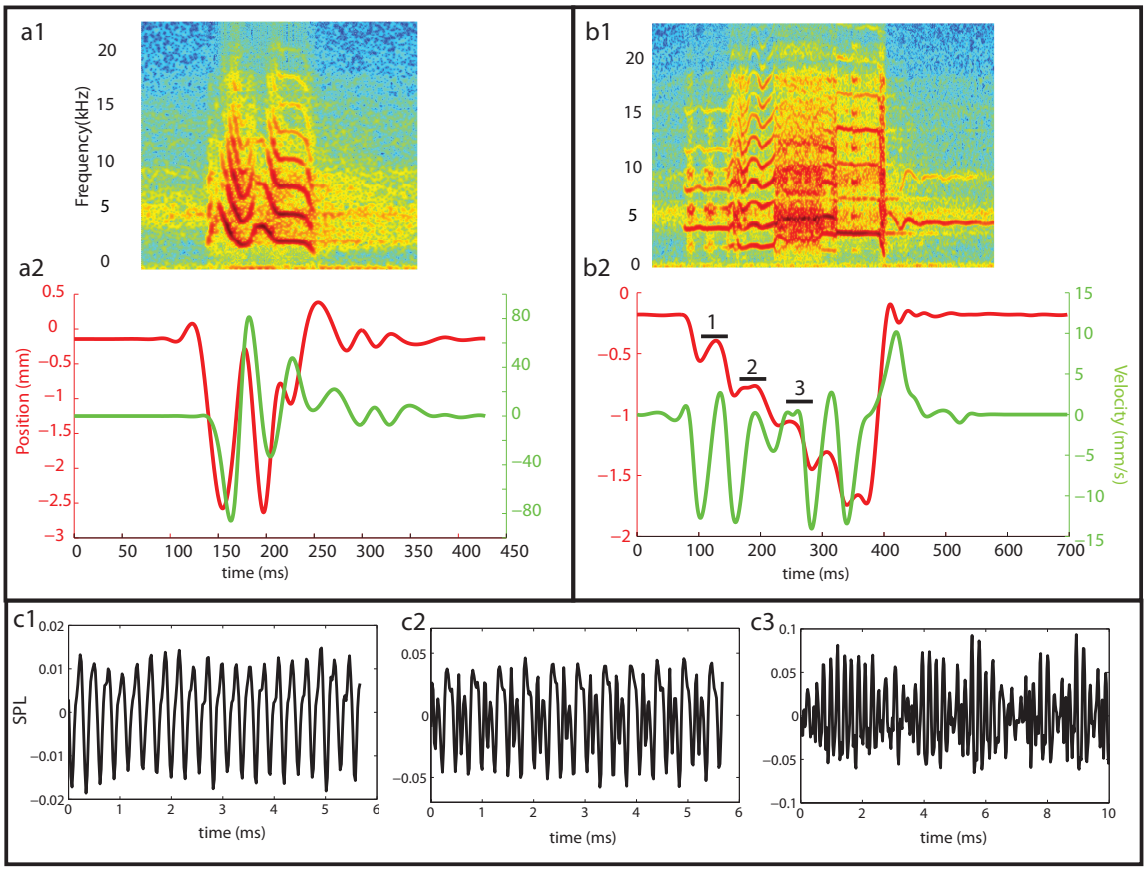

Figure 2.7: Dynamic Action of probe. (a1) and (b1) shows the spectrograms of two complicated sounds created by dynamically controlling the probe. The probe is programmed with a pulse sequence to create the sounds (we specify the position and acceleration). (a2) and (b2) show the position of the probe (red), and the corresponding velocity (green), that was used to create the sounds. (c1-3) shows the waveform for the sections indicated in (b2). c1) shows sinusoidal oscillations, c2)shows a period doubled sound and c3)shows chaotic sound. Thus by actuating the probe we can dynamically change the "kind" of sound produced.

between the solitary and chaotic phase and the probe acted a switch between the two behaviors.

Figure[8] shows spectrograms of real bird songs (top) and artificial songs (bottom) created by dynamically probing the artificial syrinx. Fig[8a1,a2,a3] shows tonal songs of the Red Eyed Vireo, fig[8b] is a song segment from a Bengalese finch and fig[8c] is a song segment from a Zebra Finch. The parameters, as mentioned before, were the static tensions applied longitudinally throughout and transversally at the mouth, flow velocity, and position of the linear motor. The vireo has a beautiful tonal song with large changes (or sweeps) in frequency. To ensure no unintentional "phase" transitions were introduced, the device was biased in an entirely tonal regime to allow large sweeps in frequency. This meant that probe had to be placed very close to the mouth (0.3 cm). The flow velocity was set at 5m/s.

The first of the songs is clearly the best copy while the others measure up to the original partially. Song [a] was relatively simple to create; in the first part the notes were just pressed and held, while in the second part the frequency was moderately swept. Note that the sweeps were not simple linear chirps but have more interesting shapes. It was not possible to control the linear motor with high enough precision, so the shape of the recreated spectrum was only approximate, but quite similar. The segment marked 1 in figure[8a1] was difficult to reproduce because of the large changes in acceleration required to create the double hump feature. On the other hand the segment marked 2 is reproduced quite well since the changes are far more gentle. The mimicked song did include some higher harmonics, as did the original song, albeit to a lesser extent. We believe that a small portion of higher modes are also excited in

the bird also and are filtered out via their acoustic filter comprising the throat and beak.

The second song (figure[8a2]) shows some very interesting features. Each segment looks like a stylized "v" with the energy concentrated on the upsweep. The reproduction was poor because it was not possible the turn the device "off" rapidly on the downsweep. As a result we did not get a series of isolated chirps but rather a continuous signal. The bird might perform this song by simultaneous gating of the airflow which would allow it turn phonation off on the downsweep. With the third song (figure[8a3]) we encountered the same difficulties as with the second song. The first part of the song comprised of a segment where each note consisted of two rapid downsweeps connected by a sharp upsweep. We succeeded in reproducing only one of these downsweeps. The second part of the song is a downward sweeping trill (at almost a 100Hz!), which implies that the bird either has muscles that can operate at a 100Hz, or the bird knows an area of phase space governed by such esoteric dynamics. We did not find such an area in phase so this segment of the song was created by rapidly modulating the linear motor rapidly but a repetition rate larger than 40Hz was not achieved.

The device was more successful in mimicking multi harmonic songs, especially that of the Bengalese Finch (Figure[8b]). To recreate this song the device was first biased deep in the solitary phase and the individual notes were creating by probing the motor to different depths. The song started with a short section of period doubled sound and then onto a series of short pulses slowly descending in frequency, and ended with a short section where the fundamental frequency of the multiharmonic song varied a

little. To produce this song the linear motor placed was 1.2cm from the mouth and the airflow set to 5m/s. The first part of the song was created by pulsing the motor to various depths depending on whether the sound was period doubled or not. The second part was created by biasing the device in the solitary phase and programing the motor such that its displacement approximately matched the changing fundamental frequency of the song. As we have shown earlier, the fundamental frequency of the sound produced by the device in this regime varies linearly with the probe depth.

The wildly varying song (Figure[8c]) of the Zebra Finch was the most difficult to reproduce because it combined the high acceleration sweeps of the vireo with sudden changes in mode structure like that of the Bengalese Finch. We break the song into 5 segments depending on the nonlinear features they exhibit. Segment 1 starts with a transition from an almost pure tone to a multi harmonic downsweep and then a rapid sweep. We could capture some of the features, but not all the rich harmonic structure. The flow velocity was set to 5m/s . Segment 2 is very complicated and shows transitions to chaos with some structure of a rapid downsweep. To mimic this section flow velocity was increased the to 7m/s to find a region in phase space where mixed solitary chaotic modes existed (please refer to Figure[3]), and applied the appropriate pulse sequence to approximate the downward sweep in frequency. Segment 3 is similar to segment 2, except there is a short wait before the downsweep, which has a slightly different shape also. Again, we can match some qualitative features but not all the diversity. In our opinion segment 4 and 5 have been best reproduced. Segment 4 starts with a rapid downsweep and then suddenly halts and holds at a particular frequency. This sudden acceleration and deceleration of the

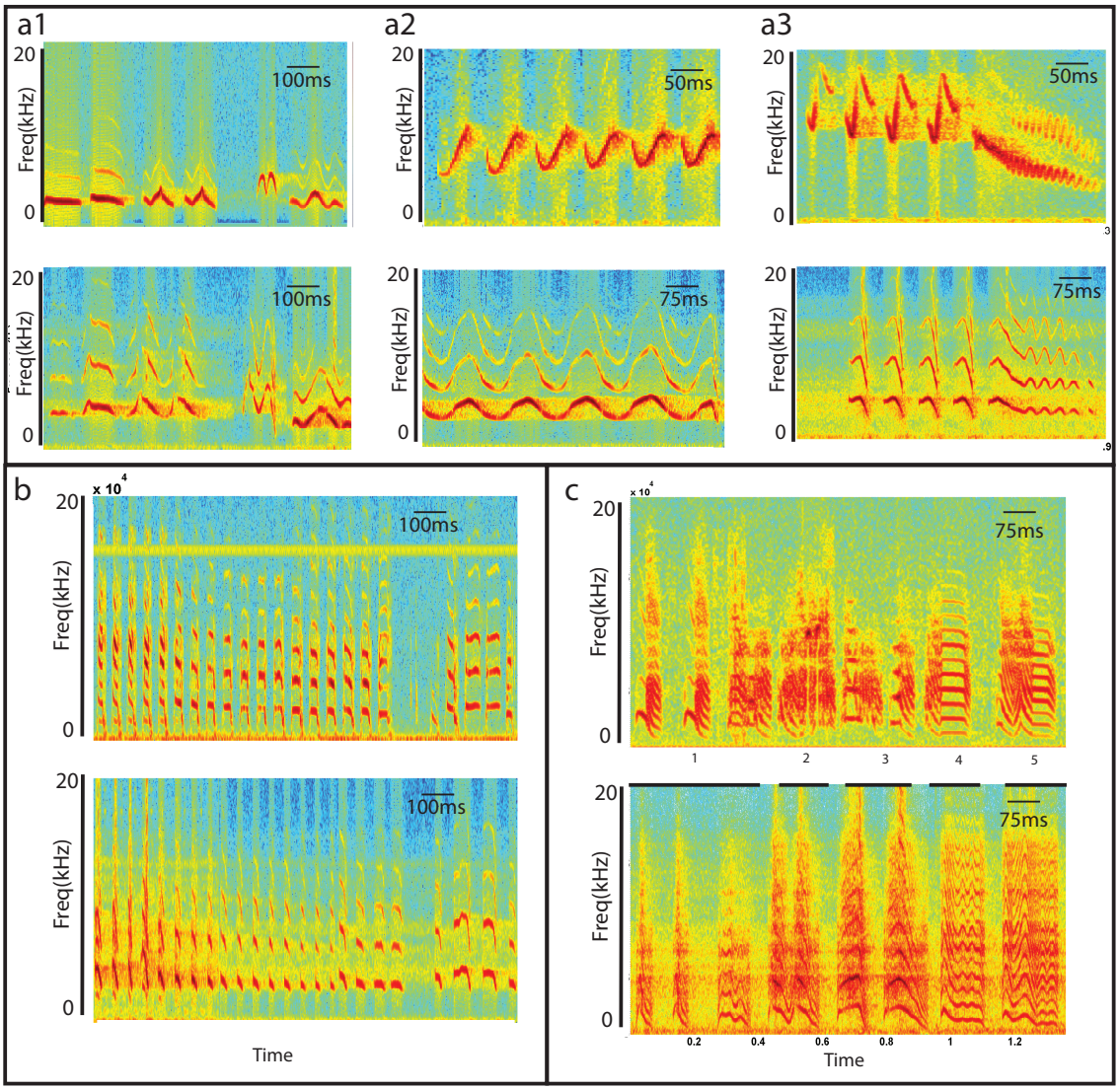

Figure 2.8: Spectrograms of real and copied bird songs. (a1-a3) Top Panel shows real bird songs from a red eyed vireo, and the bottom panel shows the copied songs created by dynamically controlling the device. The vireo has beautiful tonal songs with rapid and large variations in frequency. The device was operated in the tonal regime and reproduces songs well when the variation in frequency is not very large (a1). (b) shows a real (top) and the copied (bottom) song from a Bengalese Finch. These songs consisted of short harmonic pulses, which were well reproduced by the device. Even subtle frequency changes and transitions to a period doubled mode were well captured. (c) shows a real (top) and the copied (bottom) song from a Zebra Finch. These songs show large spectral variation as well as high harmonic content and are difficult to reproduce. However, given the limitations of the linear motor, many features of the Zebra Finch song (large changes in frequency, transitions to chaos, high harmonic content) can be qualitatively reproduced.

motor required created many undamped transient responses both from the device and the linear probe itself; as result of which the spectrogram had small undamped oscillations. In a real bird the syrinx is surrounded by thick musculature and tissues and may help in dampening out such transient modes. Segment 5 is similar except there is a down-up-down sweep at the beginning. Again the oscillations in the motor did not allow us to wait steadily at one particular frequency.

We have thus shown that to a large degree we can empirically control our device to produce sound that mimic bird song. The next step would be to apply a more robust control that done so far and investigate approaches to automated learning. This was done first mathematically with single frequency songs (this work was done by Prof. S. Mandre, and reported here for the sake of completion), by thinking of bird song as an optimization problem.Consider an oscillator

$$\ddot{x} + r(t)\dot{x} + \omega^2(t)x = 0, \tag{2.2}$$

where $x(t)$ models the acoustic signal corresponding to the song, and $r(t)$ and $\omega(t)$ are two functions that we can manipulate to generate the signal. From what we have seen so far, $\omega(t)$ and $r(t)$ (we can think of this as volume control, where negative $r(t)$ corresponds to turning the volume off) are only slowly varying functions of time. Given this piece of information the song can be cast into the language of linear optimization theory by the equation.

$$\underset{r(t),\omega(t)}{\text{minimize}} \quad \int_0^T (x - u(t))^2 + W_1 \left(\frac{d\omega}{dt}\right)^2 + W_2 \left(\frac{dr}{dt}\right)^2 dt \tag{2.3}$$

subject to $\ddot{x} + r(t)\dot{x} + \omega^2(t)x = 0$.The problem is solved using a WKB approximation

solution of the equation above In this model the damping term can be negative (decay) or be positive in order to have growth of the signal (this models the effect of the lung to produce air flow). The next natural step would be to apply such an optimal control method to try and "solve" a multi harmonic song.

In conclusion, our attempts at creating a bird song have seen some success. In the first part of this work we investigated the mode dynamics of a thin, soft, elastic cylinder and demonstrated the existence of three nonlinear modes which bear remarkable resemblance to song motifs from small song birds. Using a linear motor to mimic the squeezing action of muscles we were able to dynamically control and produce entire song segments (not just a single note) over a few species of song bird. Remakably the control was extremely simple; in most case the z-position of the linear probe was the only parameter required to create the song. This seems to suggest that the neurological control of bird song might be less complex than previously thought, with a lot of the complexity being shifted to the inherent nonlinear dynamics of the syrinx.

Chapter 3

Hydrodynamics of a spherical fish robot

3.1 Introduction

Animals that fly or swim astound us with their aerial and aquatic acrobatics. House flies hover [29], make sharp turns [28, 7, 18]; their flight maneuvers put any pilot to shame; while the effortless graceful movement of aquatic creatures [11, 5] make our ships and submarines look sluggish. The question of how these creatures perform such dazzling stunts has vexed and excited biologist, physiciscts, engineers and aerodynamicists for decades [9, 20] . Several theories exist to explain the observations, but the gross over simplification required to handle the complexity of fluid dynamics governed by the Navier Stokes equations, leaves many subtle points to be explored [20, 5]. The descriptive range of these theories depend on a parameter known as the Reynold's number which can be thought of as the ratio of inertial to viscous stresses

exerted in a fluid. Re=0 corresponds to a completely viscous fluid and Re=∞ corresponds to a fluid with zero viscosity. Theories that work at low Reynolds number are resistive i.e. thrust is generated by the drag force exerted on a small section of the creature's body in contact with the fluid. Taylor, Hancock and Gray [19] used these theories to explain the swimming of aquatic nematodes. On the other hand for flows with high Reynolds numbers there are two kinds of theories. The first of these developed by Lighthill [21] can be described as reactive, where thrust is generated by the reaction of the body to the acceleration (inertial forces) imparted to a certain body of the fluid. The second kind is a lift based theory where thrust is generated by creation of circulation much like that of an airplane wing and tries to explain the physics of flying insects and birds. However these theories can be described as being steady or quasi-steady, that is the forces generated do not depend on time. There is no net acceleration of the body since the thrust produced balances the pressure drag, skin drag or gravitational forces exerted on the animal. Animals however do not have stationary appendages. Birds and insects flap their wings, and fish fan their tails in order to generate thrust and lift. At intermediate reynolds numbers applicable to the flying of insects and swimming of small fish, recent PIV studies show a plethora of unsteady effects that can enhance thrust produced factors much larger than expect from steady or quasi steady theories.

It has been known and recently demonstrated that insects create and shed a staggering array of vortices into the wake which can lead to enhanced propulsive forces. One of the most prominent examples of exploitation of unsteady behavior is the clap and fling mechanism proposed by Weis Fogh in order to explain the flight

behavior of the hawk moth [28, 7] At the start of the wing beat cycle the insect holds its wings together tightly and lift initiates when the the two wings peel apart causing a suction of air in the gap created. As the air accelerates around the sharp edge of the wing a vortex pair is created in accordance with Helmholtz theorem; each vortex attaches to either wing throughout the entire wing cycle thus creating net circulation around a circuit that contains each wing and thus lift. It has also been observed that certain insects use their wings as an thin aerofoil with a high angle of attack. At the end of each wing beat the winds rotate rapidly (pronation) so as to always maintain a positive angle of attack and hence lift. In another mechanism proposed by Weis Fogh, [7, 4], the rapid rotation of the wing can create rotational circulation leading to lift. Use of vortices is not just limited to insects but it has also been recent shown that certain fish create and direct short jets, that are initiated by creation of vortex rings, for a fast start or a rapid turn by rapid flicks of its tail [6]. Motivated by such phenomena, in this paper we report on the design and analysis of a fish type robot that uses unsteady fluid forces in order to generate thrust. The unsteady response was elicited by impulsively moving a tail like appendage through the fluid. We found that the response was not limited to an added mass inertial reaction force but also the creation of vortex rings (dipoles in section) which abate or help the motion of the device depending on the time of its release into the free stream.

The linear dimension of the device was 5cm and the Re was 500-1500. This corresponds to the Re observed in smaller insects, but the larger fluid density of water allowed us to also use the added mass reaction force in addition to vortex forces. Fish swim in different ways, but broadly they can be categorized into two

groups: anguiliform (eels and sea snakes that swim by passing a sinusoidal wave down its length) and carangiform (such as observed in fast swimming fish such as salmon, where the largest amplitude motion is restricted to the latter portion of the body so that a full wavelength is never visible [20]. Our device was modeled after the carangiform gait, that is the caudal fin was stiff and the amplitude was smallest towards the front and largest at the end. There were certain differences however, the tail tip velocity was much slower than bending velocity of the tail, which is not the case for real fish. Slip velocities (tail velocity/ bending speed) in fish have been reported to be around 0.7 but in our system it was only 0.1; hence we observed certain differences from a true carangiform gait. Further we observed that the tail gait depended on its interaction with the fluid and behaved like a coupled dynamical system, where the output response depended sensitively on the drive frequency as will be shown below. Briefly, we found that for low frequencies the tail moved back and forth in a circular arc, while for higher frequencies the tail swept out an area in a figure eight pattern that was either symmetric or not, depending on the frequency.

Hence the goal of this project was two fold. The first, to design a device that swam freely by impulsively moving its tail. The second, to investigate the unsteady elastohydrodynamics displayed. The results showed that unsteady effects gave rise to a thrust 3 times larger than expected from steady state studies. The second goal also served as an example of passively programmable dynamics. In such an effort, the goal is to understand how to produce complex outputs by providing simple inputs, that is, in a similar vein as bird song, to find an appropriate path in "phase space" where the dynamics matches the desired output. In the device presented the simple input

was drive frequency and the output was three different gaits, one of which maximized thrust.

3.2 Device Details

The goal of the present study was to investigate the effects of unsteady fluid motion on thrust generation. Specifically we studied thrust production as function of the frequency of an impulsive force applied to fluid using a caudal tail like appendage. The tail was cut out of 10 mil thick PEEK plastic sheet ($E \sim 10^9 Pa$), rectangular along its length (length 4cm, width .5cm), with a triangular piece (area $\sim 2 \times 10^{-4} m^2$)attached to function as the caudal fin [fig 1]. The tail was actuated using a magnetic system, and was loaded as a cantilever held between two coils of radius 1cm (see figure[1a]). The coils were arranged in an anti Helmholtz configuration (distance between the coils is equal to their radius and the currents flow in opposite relative directions) such that a qudrapolar field was created between them. In the center of this coil configuration the field varies linearly with distance, so a small permanent magnet placed in the center it feels an approximately constant force given by $\vec{F} = -\boldsymbol{\nabla} B.\vec{m}$, where m is its magnetic moment. Two neodinium permanent magnets were attached to the side of the tail and the coupled tail-magnet was driven by the coil system. Figure[1b] shows an image of the prototype device used for measurement (left) and a smaller device (coil diameter=1cm) fabricated using a 3d printer [device was fabricated by Mike Tolly in the group of Prof R. Wood].

The tail was loaded a simply clamped cantilever held in the center between the coils. The permanent magnets were attached to the tail such that they lay in center of the two coils in the equilibrium position. The applied force was calibrated by measuring the tip displacement of the cantilever in a static field and gave a value $\sim .2N/A$. The impulse was provided electronically using square pulses of current to drive the coil. In order to change the direction of the applied force the direction of the current had to be reversed in both the coils, and this was achieved using a homemade H-bridge circuit. When actuated dynamically the tail behaved approximately like a doubly loaded cantilever, where the strong magnetic driving force was applied close to its center was the first load and the fluid forces acting on the tail extremity was the other. This led to interesting dynamics of the tail tip, depending on the drive frequency.

The physical parameters of the problem were, Magnetic force (0-.5N), mass ($\sim 5 \times 10^{-2} kg$), tail length ($\sim 10^{-1} m$)), tail width ($\sim 10^{-2} m$),tail thickness ($\sim 10^{-4} m$), E ($\sim 10^{9} N/m^2$), Bending moment $Et^3 (\sim 10^{-3} Nm)$. The resonance frequency of the cantilever can be estimated, $\omega_n = k_n^2 \sqrt{EI/\lambda L^4}$, where k_n is a dimensionless number depending on the mode of oscillation, I is the moment of inertia, and λ is mass per unti length. In free space we observed $f_1 \approx 8Hz$, which was close to the estimated value of 7.7Hz. In water the resonance frequency was compensated for the added mass $f_{fl}/f_{air} = (1 + \frac{\pi \rho_{fl} b}{4 \rho_{beam} h})^{-1/2}$, where b is the width of the tail and h is the thickness [15]. The virtual mass or added mass of water that the tail has to move in addition to its own mass, lowers the resonance frequency of the cantilever. We observed the resonance of the first cantilever mode to be lowered to 5Hz, and at higher frequencies

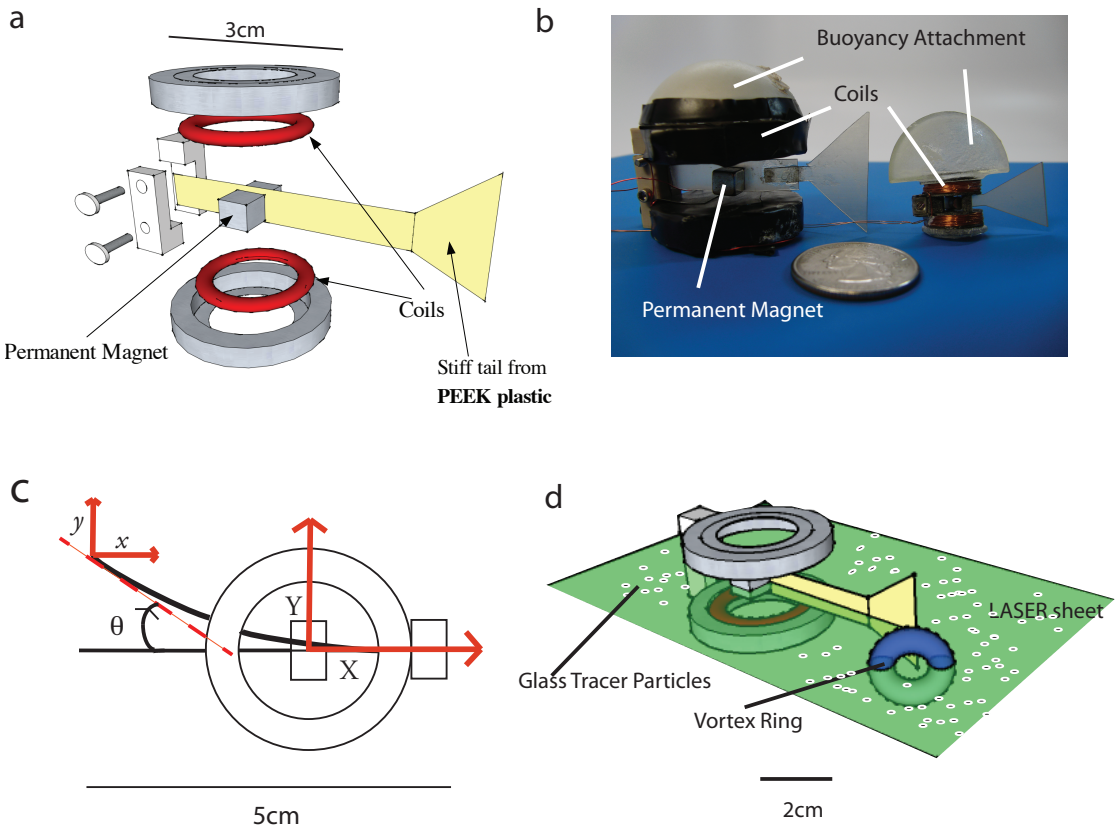

Figure 3.1: (a) Schematic of the device. The coils were arranged in an anti Helmholtz configuration and produced a qaudrapolar magnetic field.(b)Images of real devices. The device on the left is the prototype used for measurements and on the right, the device was fabricated using a 3d printer (c) Coordinate system used to describe the device indicating the dynamical variables that were extracted from the images and used for estimation of thrust and drag. (d) PIV Setup showing the plane of imaging. A 4W continuous supply Versalaser was used as the laser source and hollow glass spheres (r=10μm) were used as tracers. A schematic of a vortex ring is shown that is shed by the tail and the end of each cycle.

(>10Hz) a second mode was observed with a resonance around 16Hz. The second mode was a hybrid mode between the first and second cantilever modes, where the tail tip displayed a figure eight motion. The real second cantilever mode was observed with exceedingly small amplitude around 25Hz.

To analyze the behavior of the device the input power was kept constant and dynamics of the center of mass of the body and the tail were measured as a function of drive frequency. The experiments were performed in a tank (l=30cm, w=20cm) and imaged using a back lighting technique and imaged at 1000Hz with a Phantom V9.1 fast camera. The entire time trace of the center of mass of the body and the tail section were extracted from the images using custom software written in MATLAB, from which dynamical quantities such as linear and rotational velocities and accelerations were computed. Figure[1c] shows a schematic of the coordinate system and various dynamical variables measured.

Finally PIV analysis was performed using hollow glass spheres (r=10μm) as tracers. The laser used was a 4W continuous supply Versalaser and the analysis was done using custom software developed by Prof. M. Bandi.

3.3 Results

Fig[3a] shows the amplitude and angular response of the device as a function of drive frequency (normalized by the resonance frequency ω_0=5Hz). In free space the resonance was 8Hz and lowered to 5Hz in water. The estimated the added mass contribution from the tail was $m_{added} \sim \rho\pi d^2 L \sim 10^3 \times 10^{-6} \sim 10^{-3} kg$ which was smaller than the factor of 4 expected from the lowering in resonance frequency. Hence

this was already an early indication that the fluid accelerated by the tail was much larger expected from steady studies. We observe and explain below that the added mass of a vortex ring created during start of the tail cycle can exceed the amount expected by upto a factor of 3.

The shape of the amplitude is sufficiently different from a single Lorentzian profile as could be expected from a driven damped harmonic oscillator. However the amplitude profile fits well to a sum of two Lorentzians centered at 5Hz and 16 Hz with $\gamma = 3Hz$ and $5Hz$ (solid line in fig[2a]). The first resonance is due to the expected first mode of a cantilever; that is that tail just sweeps back and forth making a circular arc with its tail tip. However in the second mode we found, that the tail tip followed a figure eight shape. The shape is generally asymmetric but close to the resonance it seemed perfectly symmetric. It is a curious fact that the tail gait resembles that used by many hovering insects to generate lift. In this mode tail starts impulsively following the previous cycle, and after translating at a high angle of attack, for approximately half the tail cycle it undergoes a rapid rotation towards the end of the cycle. After this rapid rotation the second half of the tail cycle begins. Far from the resonance the two halves of the cycle are not symmetric; in one half the tail the axis of translation is perpendicular to the direction of forward motion and generates very little thrust and in the second, the axis is inclined at an angle and thrust is generated. Experiments performed by Dickinson [4] show that the timing and axis of rotation has a dramatic effect on the lift and drag forces generated.

The behavior of the device can grossly be categorized according to its tail trajectory (fig[2]). Close to the first resonance the tail tip follows roughly a circular arc,

makes a quick turn and retraces the arc (in the reference frame where the device is stationary). Close to the second resonance the tail describes a figure eight shape. Finally in the third regime the tail translation is small and the motion is dominated by rotation of the tail tip. Figs [2a1,b1,c1] show the time trace of the inertial force experienced by the device over two tail cycles for drive frequencies 5Hz, 15Hz and 25Hz (computed by taking the second derivative of the position of the center of mass. The top panel shows the inertial forces experienced in the X direction (See fig[1b] for reference to axis), in green, and the middle panel shows the Y component of the inertial forces, in blue, scaled by the pressure drag force on the device, $C_D \rho A \dot{X}^2$ (where the drag coefficient is taken to be 1 and A is frontal surface area). The bottom panel shows the y position of the tail tip (in red) and the angle θ made by the tangent at the tail tip with the X direction. The orange (blue) bar highlights the timing of the maximum of thrust (drag) encountered relative to tail position and angle. The solid and dashed red and black lines correspond to estimates of thrust based on translational and rotational velocities and accelerations of the tail tip. The input electric power was fixed for all drive frequencies, however the amount contributed towards thrust depended on the frequency. Intuitively one expects power transfer to be maximized at the largest resonance, but we find that the maximum output power occurs at 18Hz which is very far from resonance. We observe that at higher frequencies unsteady effects dominate allowing the tail to accelerate a much larger mass of fluid in order to transfer momentum to itself than steady or quasi steady theories predict. At 5Hz, there is a peak in thrust at the beginning of the tail cycle, and drag in the middle followed by a thrust peak again at the end of the half cycle. However the two

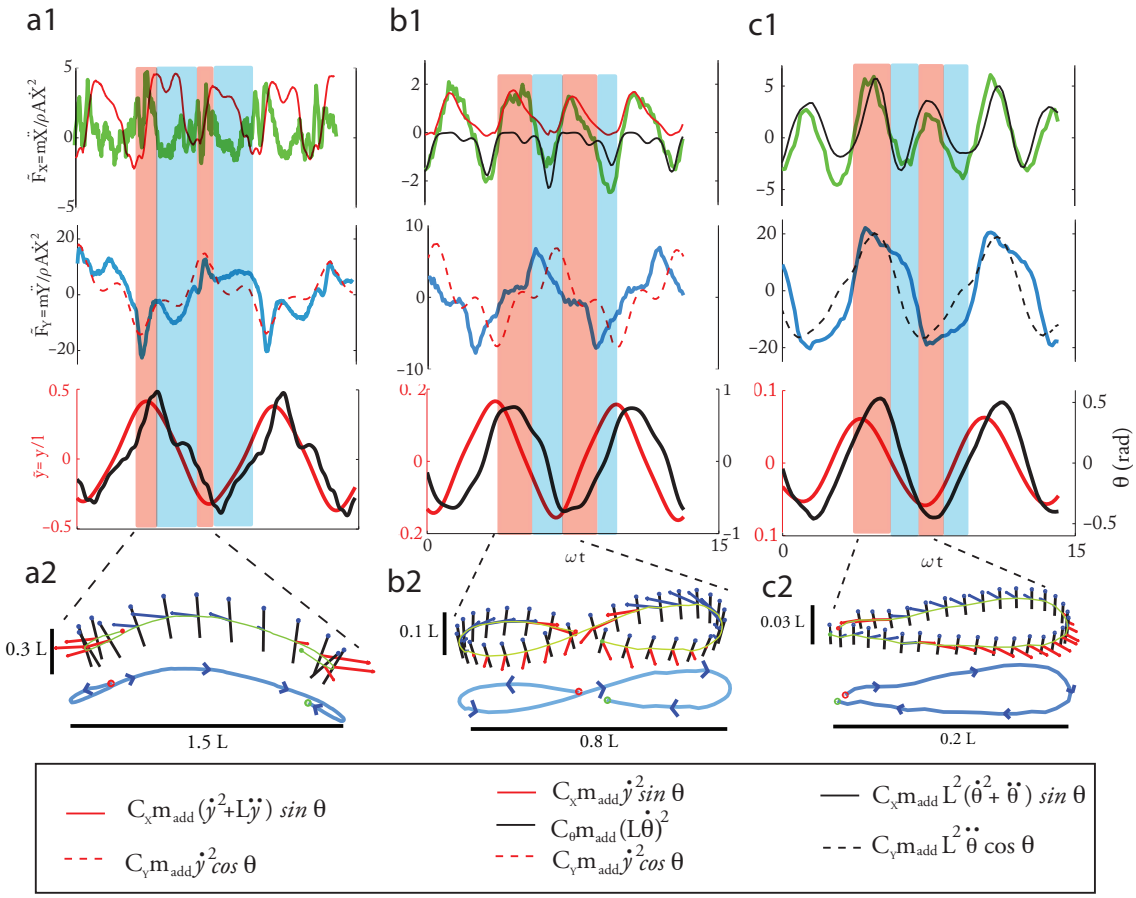

Figure 3.2: (a-5Hz, b-15Hz, c-25Hz), [a1,b1,c1]-Top Panel- (In green) Inertial force on the device in the X direction normalized by the pressure drag force $(m + m_{add})\ddot{X}/\rho A\dot{X}^2$, where m is the mass ,$m_{add}$ is the added mass due to motion of the entire device and A is the frontal area.(Solid Red) Esitmates of thrust based on tail velocity and acceleration, see Legend for expression used.(Solid Black) Contributions to thrust and drag coming from angular velocity and acceleration. For higher frequency tail angle and position are not in phase. Middle Panel-(In blue) Normalized Inertial forces in the Y directions (In dashed red and black) Estimates based on tail dynamical parameters. Bottom Panel- (In black) tail position, y and (In red) tail angle θ. [a2,b2,c2] Trajectory of the tail tip in a frame of reference stationary with respect to the device. The black lines represent the end of the tail, the tip is marked with a black circle. The red and blue arrows correspond to the inertial forces shown in [a1,b1,c1]; red indicates that the force has a thrust component and blue that there is drag. For 15Hz we find the figure eight pattern characteristic of hovering insects.

peaks are of different height thus the main thrust comes only from a small portion of the cycle. Fig [2a1] shows that the thrust peaks when the tail tip has reached it maximum position. Then as the tail reverses direction it loses thrust and the device decelerates. Since the value of the inertial force while decelerating was close to that of the expected drag force we can assume that there was no extra drag due to the wake and the deceleration was only due to the pressure drag felt by the entire device.

At 15Hz, we found a peak in thrust immediately after that tails maximum excursion. At the beginning of the cycle the tail started off at a high angle of attack for a third to a half the way after which it rapidly rotated and reversed its angle of attack for the next half cycle. In contrast to the response at 5Hz the thrust peak persisted for almost half the cycle and was followed by a peak in the drag force. Finally at 25Hz (fig[2c1]) the tail tip showed very little translation (less that .1L) and its dynamics were dominated by rotation. The tail tip position and angle were almost $\pi/2$ out of phase and the peaks in thrust correlated with the angular acceleration and the peaks in drag with angular velocity.

Estimates for the observed thrust can be made using the relation $T = .5Cm_{added}(\dot{y}^2 + L\ddot{y} + L^2\dot{\omega}^2 + L^2\ddot{\omega})$ where L is length of the tail and C is a constant quantifying the contribution due to unsteady flow (for only inertial added mass contribution C=1). In order to find the thrust in the X and Y directions the above expression was multiplied by $\sin\theta$ or $\cos\theta$. The red (black) lines in the top two panels of Figure[2-1] correspond to the contribution from tail translational (rotational) velocities and accelerations. For 5Hz the coefficients were 3, and drag was observed immediately after a peak in thrust while inertial added mass theory predicts thrust production for at

least half the cycle. At 15Hz the thrust component matches well with added mass contributions from the tail but the factor C is ∼4. The peaks in drag correlate with the angular velocity of the tail. At 25Hz no correlation was found between the thrust and translational velocities, but corresponded to angular velocities and accelerations instead with C ∼2.

Figure[2-2] shows the trajectory of the tail in a frame stationary with respect to the fish. The green line is the actual trajectory taken, and the red and green dots indicate the start and end of the trace. The black lines represent the end of the tail, the tip is marked with a black circle. The red and blue arrows correspond to the inertial forces shown in figure[2-1]; red indicates that the force has a thrust component and blue that there is drag. As mentioned above, at 5Hz the tail makes a circular arc with thrust generated at the end of the tail cycle, while for 15Hz the tail follows a figure eight trajectory with thrust being generated in the upsweeps and drag during the rapid rotations. At 15Hz the tail follows an elliptical path with drag incurred the first half and thrust in the second.

Fig [3b] shows the average velocity of the device in the X and Y directions as a function of the drive frequency normalized by the parameter $L\omega_0$, where L is the length of the device. The forward velocity (shown in blue dots) of the device increases monotonically with frequency till 18Hz after which starts to decay. The solid line is a fit of the form $\sim A\omega/\omega_0$ where A is the double Loretnzian approximation to the tail amplitude (see Figure [3a]). This shows that the forward velocity of the entire device is linearly related to the velocity of the tail. Figure[3c] shows the forward velocity divided by tail velocity (.4) and confirms this observation. The red dots in figure[3b]

correspond to the maximum velocity in the Y direction (since the mean is zero), and shows a peak close ω_0 and flattens out thereafter. Particle Image Velocimetry was

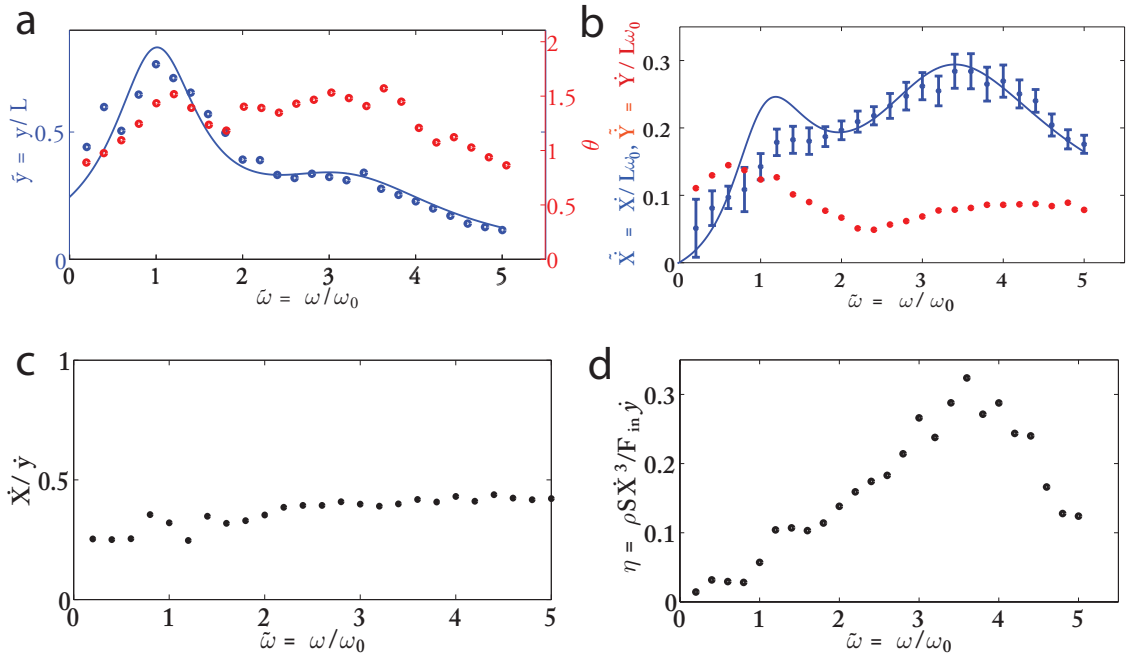

Figure 3.3: (a) Tail translational amplitude (blue dots) normalized by the length of the tail and angular amplitude (red lines). The solid lines are a fit to a double lorentzian with peaks at 5Hz and 16Hz with γ=3Hz and 5Hz. (b) Device velocity in the X and Y directions ($\ddot{X}$ and $\ddot{Y}$) normalized by the factor $L\omega_0$ (where L is the length of the device and ω_0 =5Hz) shown in blue and red dots respectively. The solid is $A\omega/\omega_0$ where A is tail amplitude (c) Forward velocity divided by tail velocity as a function of drive frequency. Above 5Hz the forward velocity varies linearly with tail velocity (d) Efficiency of motion computed as Power output against pressure drag/Power input to accelerate the fluid $=\rho S\dot{X}^3/F\dot{y}$, where F is the input driving force from the magnetic fields.

used to analyze the flow field created by the swimming the device at 6Hz, 8Hz and 12Hz. Streak images were obtained till 16Hz.Figure 4 shows flow field behind the tail for a half cycle at a drive frequency of 8Hz. At 0.0 ms, as the tail starts a new cycle a large vortex is attached to its trailing edge. The vortex creates a suction pressure

that exerts a force that acts roughly parallel to the direction of motion. Hence thrust is lost and the device is accelerated in the Y direction. However as the tail translates the vortex becomes unstable and breaks up causing a drop in the suction pressure. However some vorticity remains in order to satisfy the Kutta condition at the trailing edge. Since we are in an inviscid fluid the net vorticiy must be zero and the tip vortex is accompanied by a bound vortex of opposite circulation. At the end of the cycle the vortex dipole is released into the free stream and transfers momentum to the fluid. At the start of the next tail cycle 72-88ms the flow is directed slightly downwards and a large vortex is attached to the trailing edge. Since the tail velocity has component in the direction of swimming, dragging the fluid behind it generates thrust. The situation for the other frequencies is similar, however the exact timing of the vortex capture is different.

Figure[4b] shows the flow in the X direction in a transect behind the tail averaged over an entire tail cycle. The net positive flow indicates the generation of thrust. For 6Hz, the flow is very spread, but for 8Hz and 12Hz, the flow is more directed indicating the generation of spatially directed jets. Figure [4c] shows the flow as a function of time averaged spatially over the transcect for to tail cycles. The peaks in the time trace indicate the net transport of momentum across the transect. For 6Hz and 8Hz there is only one peak per cycle indicating that only of of the emitted jets contributes to thrust. For 12Hz we see the beginnings of a second peak in momentum transport, at the end of the cycle.

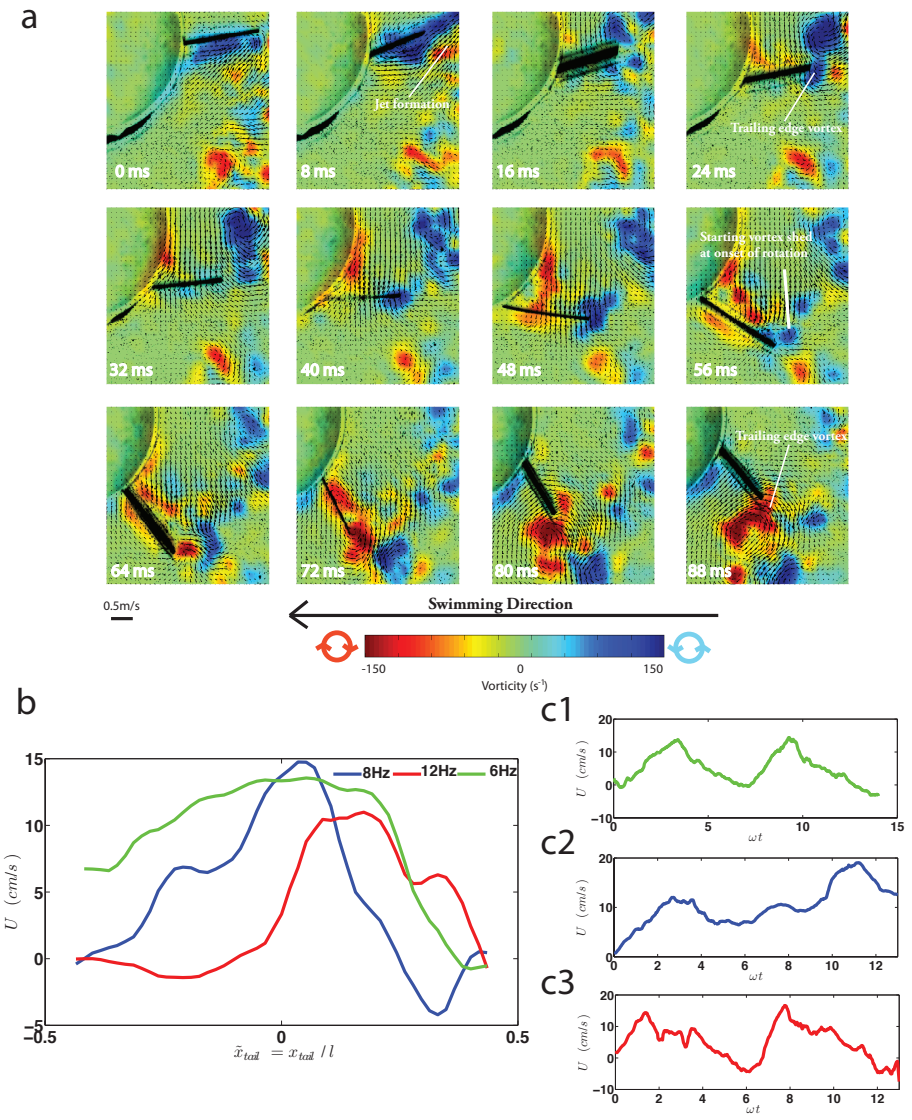

Figure 3.4: (a) PIV images of half tail cycle at drive frequency of 8Hz. At 0ms a large trailing edge vortex can be seen, which can be enhanced by vortex capture from the previous cycle. The tail moves vertically first and does not produce any thrust. However at the beginning of the next half cycle the flow shows a component in horizontal direction and hence generates thrust. (b)Flow in the X direction in a transect behind the tail averaged over an entire tail cycle. The net positive flow indicates the generation of thrust. For 6Hz, the flow is very spread, but for 8Hz and 12Hz, the flow is more directed indicating the generation of spatially directed jets. (c) Flow in the X direction as a function of time averaged spatially over the transcect for to tail cycles. The peaks in the time trace indicate the net transport of momentum across the transect. For 6Hz and 8Hz there is only one peak per cycle indicating that only of of the emitted jets contributes to thrust. For 12Hz we see the beginnings of a second peak in momentum transport, at the end of the cycle.

3.4 Discussion

Quasi steady aerodynamics tells us that lift based forces arise when a starting vortex has been released from the body in translation. The drag force traditionally applies to the pressure drag of the fluid flow behind the body and lift forces arise due to bound circulation created in the wing. However in the case of sudden accelerations, the starting vortex does not detach from the foil immediately. It has been reported that it takes up to 5 chord lengths for the lift to achieve its maximum value [28, 5]. This is known as the Wagner effect. In this case the lift component is small but drag is large because the attached vortices create a low pressure region behind the tail. This effect can be augmented by creation of a leading edge vortex at the tail tip. The vortices entrain fluid with it thereby incurring a drag force, and can be thought of as the "added mass" of the vortex. In the set of experiments described above we find that the drag component of the forces that arises due to the wagner effect is one of the main components of thrust for the entire device. There is also a second effect that may occur, in which more circulation is generated due to unsteady effects of rapid acceleration and can generate more lift than predicted by the Wagner effect. This phenomenon known as delayed stall [28, 5] can explain the large transient lift coefficient experienced by an aerofoil at a high angle of attack when impulsively started. We observe a large trailing edge vortex on the tail, but it was not clear whether it was generated as an unsteady effect or due to capture of the stopping vortex shed in the previous cycle (the stopping vortex of the previous cycle and the starting vortex from the present cycle have the same direction of vorticity and when captured enhance the total vorticity of the trailing edge vortex).

For animal swimming in an inviscid fluid, it was hypothesized that the source for most of the thrust was from the reaction to accelerating an added mass amount of fluid. However the subsequent shedding of vorticity and creation of the wake was considered a wasteful process and was not attributed to generating thrust. We find that the tail wake interaction considerably enhances the thrust generated from what was predicted by the old theory. At lower frequencies the tail behaved like an aerofoil started from rest impulsively. From the PIV analysis we found a large trailing edge attached to the tail tip as it started to translate. This vortex remained attached to the tail tip and created a suction pressure. The direction of the force of the vortex on the areofoil depends on the relative position of the vortex. The vortex also entrains surrounding fluid that was initially at rest. The kinetic energy imparted to the fluid comes at the expense of the input power from the tail, and hence the entrained fluid generates a drag force that acts parallel to the direction of motion. In the initial phase of the tail beat the tail is angled such that the drag force has a component in the direction of swimming motion. Soon after startup the trailing edge vortex becomes unstable and the suction pressure drops. Halfway through the tailbeat the tail moves roughly perpendicular to direction of swimming, and the thrust generated drops. As the tail angle crosses zero, the trailing edge vortex is shed into the free stream. Since the vortex is left behind the tail, a low pressure zone is created and the entire device is sucked back. This deceleration peak is obeserved before a thrust peak for all the frequencies. Once the bound vortex is also shed into the free stream (this happens at the end of the tail cycle), a small jet flow is created, and the component of the jet force in direction of swimming provides thrust to the device. Further, if the tail starts

its new cycle before the jet has completely passed, it may generate added thrust by redirecting the momentum flux created by the jet. This phenomenon is called wake capture and has been reported in [28].

As shown in figure[2a], at 5Hz the peaks in both $\ddot{X}$, $\ddot{Y}$ are correlated with the end of the tail cycle, indicating the presence of this jet. The thrust in the Y direction $\sim \ddot{Y}$ was much larger implying (and also confirmed from PIV) that jet moved mostly laterally. At the start of the new cycle the leading edge vorticity can be enhanced by the capture of the stopping vortex shed in the previous half cycle (it was not clear what mechanism gave rise to delayed stall at the beginning of each cycle). This enhancement leads to a temporary increase in the fluid being entrained by the tail, but also to an increase in suction pressure (the direction of this force depends on the relative position of the vortex to the motion of the tail). The peak in thrust observed at the start of the tail motion is often ascribed to an inertial response to accelerating the fluid. For 5Hz we find a force of .1N in the X direction and .2N in the Y direction. The acceleration forces due to added mass of the tail can be estimated as $\rho\pi d^2 L(\ddot{x} + \ddot{y}) \sim 0.07N$, where d is the height and L the length of the tail fin. Hence we find that at the start the estimates of added mass inertial response are about four times smaller than the actual forces observed (further we have also neglected the pressure drag forces acting on the device). After the initial burst, the tail maintained a constant velocity. For this phase the added mass estimates come from fluid laterally displaced by the tail [21] and can be estimated to be $\frac{1}{2} m_{added} w^2$, where $w = \dot{y} + \dot{X} \tan\theta$ [20]. At 5Hz, $\dot{X} \sim 15cm/s$ and $\dot{y} \sim 40cm/s$, which gives a mean thrust force 0.03N. This is close to the pressure drag force experienced by the

device at 5Hz, but the device is also accelerating in the Y direction, so the amount of thrust from added mass does not account for all the energy expended by the device.

The situation is even clearer for 15Hz, where the thrust force from the added mass component is a factor 4 smaller than either the observed inertial forces in the X and Y directions. However, for 15Hz we do observe a strong correlation of the the thrust to $C\frac{1}{2}m_{added}\dot{y}^2$, where the factor C is about 4. This is consistent with the theory that thrust from added mass is augmented by the drag force generated by the fluid entrained by the trailing edge vortex. The force in this case also scales with $\dot{y}^2$ so it is difficult to separate the contribution from the added mass term. In fact we can think of the vortex amplifying the added mass effect. It is also interesting that at 15Hz the tail tip makes a figure eight pattern, which is the gait adopted by many insects that hover. If we look at the device from behind (change coordinates from X$\rightarrow$-X) as it swims, the tail has a positive angle of attack and its gait looks identical to a hovering pattern. We also observed via streak images that two fully developed jets formed behind the device , implying an efficient transfer of momentum in generating thrust against the pressure drag force (which in analogy to hovering, can be thought of as gravity). For lower frequencies fully formed jets were not observed, the fluid was shed into the free stream as unlinked vortex rings. Further, since the tail reverses direction and starts the new cycle before the jet has passed it can be hypothesized that thrust can be generated by pushing off the jet and redirecting its momentum. Thus there are three mechanism via which the device generates thrust, first the acceleration of an added mass amount of fluid, second the drag force exerted by fluid entrained by the trailing edge vortex and third, momentum transfer by creation and redirection

the flow of the jet created by the start/stop vortices. It was difficult to separate out the contributions of each individual phenomenon because the all occur at the same time.

Pressure drag on the device is not the dominant source of drag in this system. The main source of comes from the suction pressure (or lift force) created at the moment the starting vortex completely detaches from the tail and a jet flow initiates between it and the stopping vortex that is still attached to the tail. Observations reveal that drag initiates at the onset of rapid rotation of the tail at the end of its cycle. PIV imaging revealed that as the tail stopped translating and started rotating, that starting vortex was finally shed, and upon the end of rotation the stopping vortex (figure[4]). Only when the stopping vortex was shed into the free stream that momentum was transferred to the device in a favorable direction .

In conclusion we demonstrated the use of a magnetic system to impulsively drive thin aerofoil at a high angle of attack, and use the unsteady response from the fluid to generate larger thrust than expected from steady state studies. Measurements of the dynamics of the swimming device reveal acceleration forces far in excess of that predicted by steady state theories. The thrust was augmented by drag forces, initiated by an attached vortex dipole created at startup, incurred by the moving aerofoil. The passive dynamics of the aerofoil were modified by its interaction with the fluid; maximum thrust was generated when the tail of the device followed a figure eight pattern, a gait, much like that used by hovering insects.

Bibliography

[1] J Brackenbury. Aeroacoustics of the vocal organ of birds. *Journal of Theoretical Biology*, 1979.

[2] R. Casey and A. Gaunt. Theoretical models of the avian syrinx. *Journal of Theoretical Biology*, 7:45–64, 1985.

[3] O.N. Larsen C.P.H. Elemans, M. Muller and J.L. van Leeuwen. Amplitude and frequency modulation control of sound production in a mechanical model of the avian syrinx. *The Journal of Experimental Biology*, 212:1212–1224, 2009.

[4] MICHAEL H. DICKINSON. The effects of wing rotation on unsteady aerodynamic performance at low reynolds numbers. *The Journal of Experimental Biology*, 192:179–206, 1994.

[5] MICHAEL H. DICKINSON. Unsteady mechanisms of force generation in aquatic and aerial locomotion. *AMER. ZOOL.*, 36:537–554, 1996.

[6] G Lauder E Tytell. Hydrodynamics of the escape response in bluegill sunfish, lepomis macrochirus. *The Journal of Experimental Biology*, 211:3359–69, 2008.

[7] C.P. Ellington. The aerodynamics of hovering insect flight iv:aerodynamics mechanisms. *Proceedings of the Royal Society of London: B*, 305:79–113, 1984.

[8] M. Fee. Measurement of the linear and nonlinear mechanical properties of the oscine syrinx:implications for function. *Journal of Comparative Physiol A*, 188:829–839, 2002.

[9] F.E. Fish and G.V. Lauder. Passive and active flow control by swimming fishes and mammals. *Annu. Rev. Fluid Mech*, 38:193224, 2007.

[10] N.H. Fletcher. Bird song, a quantitative acoustic model. *Journal of Theoretical Biology*, 135:455–481, 1988.

[11] G.Lauder and E. Tytell. Hydrodynamics of undulatory propulsion. *Fish Physiology*, 23:425–68, 2005.

[12] C.H. Greenwalt. *Bird Song: Acoustics and Physiiology*. 1968.

[13] P. Holmes. A nonlinear oscillator with a strange attractor. *Philosophical Transactions of the Royal Society of London. Series A*, 292:419–448, 1979.

[14] R. Kamm A. Shapiro I. Kececioglu, M. Mclurken. Steady supercritical flow in collapsible tubes. part 1. experimental observations. *The Journal of Fluid Mechanics*, 109:367–389, 1981.

[15] Paul Mulvaney James W. M. Chon and John E. Sader. Experimental validation of theoretical models for the frequency response of atomic force microscope cantilever beams immersed in fluids. *J. Appl. Phys*, 87:3978, 2000.

[16] O.N. Larson and F. Goller. A new mechanism of sound generation in songbirds. *Proceedings of the National Academy of Sciences*, 94:14787–14791, 1997.

[17] O.N. Larson and F. Goller. Direct observation of syringeal muscle function in songbirds and a parrot. *The Journal of Experimental Biology*, 205:25–35, 2002.

[18] Fritz-Olaf Lehmannl. The mechanisms of lift enhancement in insect flight. *Naturwissenschaften*, 91:101–122, 2004.

[19] J. Lighthill. Note on the swimming of slender fish. *The Journal of Fluid Mechanics*, 9:305, 1960.

[20] J. Lighthill. Aquatic animal propulsion of high hydromechanical efficiency. *The Journal of Fluid Mechanics*, 44:265–301, 1970.

[21] J. Lighthill. Large-amplitude elongated-body theory of fish locomotion. *Proceedings of the Royal Society of London: B*, 179:125–138, 1971.

[22] B. Pesaran M. Fee, B.Shraiman and P. P. Mitra. The role of nonlinear dynamics of the syrinx in the vocalizations of a songbird. *Nature*, 395:68–72, 1998.

[23] M.Shimizu and Y.Tanida. On the mechanism of korotkoff sound generation at diastole. *The Journal of Fluid Mechanics*, 127:315–339, 1983.

[24] D. Cugell J. Grotberg N.Gavriely, T. Shee. Flutter in flow-limited collapsible tubes: a mechanism for generation of wheezes. *Am. Physical Society*, 89:2251–2261, 1989.

[25] O.E.Jensen. Instabilities of flow in a collapsed tube. *The Journal of Fluid Mechanics*, 220:623–659, 1990.

[26] P.J.Holmes and D.A. Rand. Bifurcations of the forced van der pol oscillator. *Quarterly of Applied Mathematics*, 35:495–509, 1978.

[27] T.J. Gardner R. Laje and G.B. Mindlin. Neuromuscular control of vocalizations in birdsong: A model. *Physical Review E*, 65:051921, 2002.

[28] Sanjay P. Sane. The aerodynamics of insect flight. *The Journal of Experimental Biology*, 206:4191–4208, 2003.

[29] B.Newman S.Savage and D Wong. The role of vortices and unsteady effects during the hovering flight of dragonflies. *The Journal of Experimental Biology*, 83:59–77, 1979.

[30] Magnasco R. Laje T.J. Gardner, G. Cecchi and G.B. Mindlin. Simple motor gestures for birdsongs. *Physical Review Letters*, 87:208101–1, 2001.